Title

Dissection of the impact of tissue context on anti-cancer drug activity through the use of high dimensional combinatorial microenvironment analysis

Author

Lin, Chun-Han

Publication Date

2016

Peer reviewed|Thesis/dissertation

Dissection of the impact of tissue context on anti-cancer drug activity through the use of high dimensional combinatorial microenvironment analysis

By

Chun-Han Lin

A dissertation submitted in partial satisfaction of the

requirements for the degree of

Doctor of Philosophy

in

Comparative Biochemistry

in the

Graduate Division

of the

University of California, Berkeley

Committee in charge:

Dr. Mark LaBarge, Co-chair

Professor Andreas Stahl, Co-chair

Professor Fenyong Liu

Professor Gertrude Case Buehring

Spring 2016

Abstract

Dissection of the impact of tissue context on anti-cancer drug activity through the use of high dimensional combinatorial microenvironment analysis

by

Chun-Han Lin

Doctor of Philosophy in Comparative Biochemistry

University of California at Berkeley

Dr. Mark LaBarge, Co-chair

Professor Andreas Stahl, Co-chair

Breast cancer alone accounts for 29 % of all new cancer diagnoses and is the second leading cause of cancer related death. Improvement in early detection and the understanding of oncogenic drivers connected to malignant transformation and cancer progression has lead to an overall decrease in breast cancer related mortality[1]. However, therapeutic durability remains a problem for both chemotherapies and pathway-targeted drugs. Furthermore, the poor translation from pre-clinical screening results to clinical outcomes impedes therapeutic development.

Genomic heterogeneity and other cell intrinsic mechanisms are commonly examined as a major source of therapeutic failure. Using a reductionist approach, I examined the hypothesis that the tissue microenvironment is a potent modulator

of drug activity and therapeutic response. I first tested the hypothesis that matrix rigidity of microenvironments can modulate the efficacy of the targeted-therapeutic small molecule, lapatinib, in HER2-amplified breast cancer cell lines. The anti-proliferative effect of lapatinib was inversely proportional to the elastic modulus of the adhesive substrates. The modulus-dependent lapatinib responses were eliminated with treatment of mechanosensing inhibitors, Y27632 and blebbistatin. Knockdown of the hippo pathway mechanotransducer, YAP, eliminated the modulus-dependent lapatinib responses, and pharmacological inhibition of YAP phenocopied the effect of YAP knockdown. Reduction of YAP *in vivo* in mice also slowed the growth of implanted HER2-amplified tumors, these showing a trend of increasing sensitivity to lapatinib as YAP decreased. Thus, I addressed the role of stiffness in resistance to, and efficacy of, a HER2 pathway-targeted therapeutic via the mechanotransduction arm of the hippo pathway.

In order to dissect and investigate the microenvironmental impact on drug responses, we developed the MicroEnvironmental microarray, (MEArray) platform. The method allows for simultaneous control of the molecular composition and the elastic modulus. Utilizing the MEArray, I further tested the hypothesis that in addition to matrix rigidity, molecular composition can modulate lapatinib responses. I systematically quantified the microenvironmental impact on cellular morphological changes and the lapatinib responses. The results were consistent with our previous report that matrix rigidity conferred lapatinib resistance. I also identified that cells adhered to fibronectin showed higher

lapatinib resistance independent of stiffness. The validations showed that fibronectin conferred nuclear YAP translocation, which may explain partly the mechanism of the lapatinib resistance. Further studies for elucidation of fibronectin-induced lapatinib resistance are needed. However, simultaneous modulation of stiffness and molecular composition revealed a continuum of drug responses resulting from cell-microenvironment interactions.

Dedication

To

My Mother

My Sisters

My Brother

My Father

And

My Wife

I LOVE YOU ALL.

Acknowledgements

I want to thank my whole family, who support me pursuing my PhD. I also want to thank all the past and the present members of the LaBarge lab for their help. This work was supported in part by Government Scholarship for Overseas Study from Ministry of Education, Taiwan (R.O.C).

Table of Contents

Chapter 1: Introduction

1.1. Breast cancer and the challenges of therapeutic durability.

Cancer is the second leading cause of death in United States and it is also a general public health problem worldwide[1]. Depending upon the tumor characteristics, and patient preference, the standard treatments for breast cancer include surgery, radiation, chemotherapy, immune therapy, hormone therapy, and pathway-targeted therapy[2]. For early breast cancer, breast-conserving surgery followed by radiation provides long-term survival similar to mastectomy[2]. Once the tumors progress to later stages, chemotherapy and targeted therapy may provide additional defense against the primary tumor and prevent metastasis. Molecular subtypes of breast cancer have been investigated and used for planning treatments and developing new therapies. Depending upon the gene expression profiles of breast cancers, there are several major subtypes, including luminal A, luminal B, HER2 over expression, triple negative basal-like, and normal-like[3]. Based on clinical applications, breast cancers can be classified into three subtypes; estrogen receptor (ER) positive, HER2 positive, and “triple negative” breast cancers that do not expression estrogen, progesterone, or HER2 receptors[3]. Current major treatment strategies target only these three major subtypes. However, breast cancer is highly heterogeneous and the anti-cancer drug responsiveness varies among patients in the same subtype. Even in one patient, primary and recurrent tumors also respond differently to the same therapy[4]. Drug responses are influenced by multiple factors, such as the genetic

background, drug accessibility, and tumor microenvironment. It has been shown that the efficacy of anti-cancer drugs are lost during the transition from *in vitro* drug screening to *in vivo* animal models[5]. Also, it has been shown that conventional monolayer cultures are not representative of physiologic conditions[6]. This lack of similarity to physiologic conditions may explain why during drug development, only a small percentage of leading candidate compounds enter animal model testing, and even fewer enter clinical trials. In order to improve the rate of successful translation from pre-clinical to clinical, the impact of tumor microenvironment to therapeutic efficacy needs to be considered.

1.2. The mechanisms of lapatinib resistance in HER2 overexpression breast cancers.

Human epidermal growth factor receptor 2 (HER2)-positive breast cancers account for about 15-20% of breast cancers, have poor prognosis, and are less responsive to hormone treatment than HER2(-) breast cancers[3, 7]. Although HER2-targeted therapies are one of the success stories in breast cancer treatment[8], generating a durable drug response remains a challenge[9]. Trastuzumab, one of the major HER2-targeted therapies, is considered standard treatment for HER2(+) breast cancer and may be given together with chemotherapy to improve outcome[10]. Unfortunately, resistance to trastuzumab often occurs[11]. The tyrosine kinase inhibitor lapatinib is a potent inhibitor of catalytic activity of both epidermal growth factor receptor (EGFR) and HER2[12]; and lapatinib is often given as one of the options for overcoming trastuzumab resistance[11]. Most tumor cells with elevated HER2 levels show high sensitivity to

growth inhibition by lapatinib, but resistance often develops[13].

Several mechanisms of lapatinib resistance have been reported, including compensatory activation of parts of the HER network. Compensatory up-regulation of HER3 activation, driven by Akt (Protein kinase B) activity, confers resistance to lapatinib in HER2-amplified breast cancer cell lines[14]. Incomplete inhibition of EGFR results in heregulin-driven feedback that sustains EGFR activation, which contributes to lapatinib resistance in HER2(+) breast cancers[15]. Other mechanisms include activation of other redundant survival pathways; for example, up-regulation of the membrane tyrosine kinase AXL (Ark and Ufo) sustains PI3K/Akt signaling, conferring lapatinib resistance[16]. Hepatocyte growth factor (HGF) activation of hepatocyte growth factor receptor (MET) also is associated with resistance to lapatinib in HER2(+) gastric cancers[17]. These studies suggest that the activation of redundant survival pathways can be induced, either intrinsically, or extrinsically, by microenvironmental factors, such as growth factors.

1.3. The role of mechanosensing pathway and YAP (Yes-associated protein 1)/TAZ (PDZ binding motif) in breast cancer and therapeutic responses.

Compared to the well-known molecular compositions of microenvironment, such as growth factors and cytokines, the mechanical properties of microenvironment are less well studied. Stiffness of culture substrate has been shown to alter cell proliferation, morphology, and cell fate decisions in multipotent progenitors[18-20]. In clinical applications, it's known that tumors can be diagnosed by palpation due

to the hardness of tumor compared to adjacent normal tissue. Perhaps accordingly, breast cancer cell lines exhibit increasingly malignant and invasive behavior in matrices that are stiffer than normal breast tissue[21].

The biophysical properties of tumors change during progression, which also impacts tumor cell functions. So in addition to redundant signaling pathways, using integrin-blocking antibodies to alter how tumor cells perceived their microenvironments was shown to modulate the efficiency of cytotoxic agents[22]. Use of an *in vitro* approach, which compared responses of a number of HER2-targeted therapeutics (including lapatinib) in multiple HER2-amplified cell lines, revealed that cells were more sensitive to lapatinib in 3-D Matrigel, when compared to 2-D cultures using tissue culture plastic (TCP)[23]. Even in the relatively simplified 3-D Matrigel cultures, there are multiple chemical and physical properties that contribute to those microenvironment-dependent drug responses. Accumulating evidences suggest that microenvironment rigidity can promote tumor progression and survival through activation of growth factor signaling pathways, by enhancing integrin clustering and focal adhesion assembly[24, 25], or through modulation of microRNA expression[26]. The impact of tissue stiffness to chemotherapeutic response has been reported in a model of hepatocarcinoma, in which the cells proliferated more slowly on softer surfaces and were thus less susceptible to the cytotoxic agents[27]. The underlying molecular mechanisms of how cells sense and respond to the stiffness of microenvironment are still not completely understood. Moreover, it is not clear whether stiffness also alters the response of pathway targeted-drug therapies

that are less reliant upon proliferation for efficacy.

The Hippo signaling pathway was discovered in Drosophila melanogaster; it controls organ size by regulation of cell proliferation[28]. The control of tissue growth requires a proper kinase cascade of the Hippo pathway, composing by components such as Sav1, NF2, MST1/2, LATS1/2, YAP/TAZ, and other kinases in mammalian cells[29]. Hippo pathway is conserved in mammals as well, and is more complex than that of Drosophila. It was linked to human cancer for the first time in 2002[30]. An increasing number of studies have provided evidence to suggest that Hippo pathway perturbation and altered expression of subsets of Hippo pathway components can contribute to tumorigenesis[31]. The Hippo pathway is regulated by various signals, such as cell-cell contact[32, 33], cellular energy stress[34], and mechanical cues[35]. Under physiological or pathological conditions, these various microenvironmental signals may regulate many cellular functions, including cell fate decision, proliferation, and tumor progression, by regulating YAP/TAZ activation[36]. Breast cancer transformation has been shown to accompany by an increase in collagen decompositions; and the more aggressive breast cancer subtypes have been correlated with higher nuclear (activated) YAP and highest stiffness[37]. Although YAP has recently been shown to function as both proto-oncogene and tumor suppressor depending on the cellular context, a the comprehensive understanding of this complicated network of the YAP pathway needs further study to be elucidated[38]. The connection between mechanosensing pathway and Hippo pathway has already been shown to play important role in tumor progress[38] and therapeutic responses[39]. As such,

YAP/TAZ have become appealing therapeutic targets as alternative or combined treatments with current therapeutic strategies[40].

1.4. A failure to predict efficacy.

In anti-cancer drug development, a lackluster ability to predict how molecules will perform in humans based on pre-clinical drug screening delays the progress of drug discovery. In the last few decades tremendous resources have been invested in translating pre-clinical anti-cancer compounds into drugs approved for clinical use .However, most drugs never end up being approved for clinical use, which further elevates the cost of development, and make drugs less affordable[41].

Advancements in cell and molecular biology, and engineering have reinvented modern pharmacology, which tries to identify compounds with potentially selective activity against tumors in cell-based high-throughput screening (HTS), and then further validate the drug efficacy in animal model systems, of which rodents are the most popular. These candidates often show promising effects in lower animals, but show much less success in humans. Unfortunately, almost 70% of new drugs fail at phase II trial because they meet safety standards established in phase I trials, but exhibit no efficacy in phase II[42]. Studies have started to address the possible mechanisms involving the different expressed genomes of mice and men, and there are other significant differences that arise at the level of physiology and tissue architecture that can impact drug responses as well[23].

The tumor microenvironment, i.e. the sum of cell-cell, cell-ECM, cell-soluble factor interactions and the physical properties and geometry, has been shown to

alter cancer progression, drug responses, and a number of other tumor properties[43, 44]. Thus, an important challenge that is being undertaken in drug development is to identify pre-clinical screening modalities that take microenvironment into account and that are generally more reflective of the biology of human tissues, in order to provide a more predictable clinical outcome.

1.5. Tumors are heterogeneous "organs", and tumor microenvironments are important determinants in therapeutic responses.

The natural inter- and intra- tumor heterogeneity is thought to be a major component of drug resistance. Our knowledge of the molecular underpinnings of tumor biology has accelerated remarkably over the past two decades. The Cancer Genome Atlas (TCGA) program has identified a broad range of recurrent gene mutations and structural rearrangements that putatively drive tumor genesis, and a number of drugs have been selected to target protein changes resulting from those specific gene mutations. Many of these pathway-targeted anti-cancer agents successfully inhibit the growth of tumor cells in the lab setting, and even show efficacy in rodent models, but there is a lack of activity in actual humans[45]. More recently a nuanced view of tumors has begun to emerge viz. that they are not just a homogeneous expansion of neoplastic cells, but instead are abnormal organs, comprising multiple cell types and dynamic extracellular matrix (ECM)[46]. These "organs" interact with the body via unique vascular systems and changes in immune homeostasis that lead to evasion of immune responses as well as cancer treatments[47]. The combinations of ECM, growth factors, cytokines, tensile force, and oxygen tension contribute to control the malignant progression,

metastasis, and drug responses[44, 48-50].

The cancer stem cell (CSC) hypothesis offers attractive explanations for generation of heterogeneity within tumors, metastatic dissemination, and resistance to therapy. The underlying logic is modeled on normal developmental hierarchies that are delineated for a number of adult tissues. Undifferentiated stem cells give rise to less potent progenitors, which produce the most specialized cells of a given tissue. Analogously, only CSCs are thought capable of self-renewal, of initiating tumors at primary and distant locations, and of giving rise to more differentiated daughters that are incapable of reestablishing the tumor. Normal stem cell activity is maintained in niches; therefore, employing the same logic used for developmental hierarchies, niches that maintain CSCs, should also exist (reviewed in refs. [51-53]). Niches are specialized microenvironments, wherein stem cells reside (reviewed in refs. [54, 55]), which exert control over cell function. It was shown that progenitors both in skin and skeletal muscle could adopt residency in vacated stem cell niches, where they reacquired stem cell traits[56-58]. Impressively, testis and neural stem cells from male mice were shown to give rise to lactating mammary glands when transplanted into the mammary fat pad[59, 60]. And in true reductionist models that used defined microenvironments, embryonic and adult stem and progenitor cell fate decisions were shown to be quantifiably flexible in response to combinatorial microenvironments[61-64]. The ability of the niche to determine the functional spectrum of stem cell activities led us to hypothesize that stem cell niche microenvironments beget stem cell functions[65]. Due to their role in maintaining

stem cell activity, disrupting CSC-niche interactions may be crucial for overcoming barriers to therapeutic resistance[66]. Thus, understanding the interactions between tumor microenvironments and cancer cells is important for the identification of drug controllable mechanisms (e.g. proliferation, differentiation, and quiescence, etc.) regulated by tumor microenvironment and for improving drug efficacy in humans.

1.6. Deconstructing tumor microenvironments into experimentally tractable combinations.

Tissues are collections of cells and ECM organized into unique spatial configurations that collectively carry out specialized functions. Remarkably, tissues with an intact architecture can maintain many basic functions in spite of the presence of gene mutations that cause dysfunctions when introduced into cells on tissue culture plastic[67]. Studies showing that wound-healing microenvironments unleash malignant potential demonstrated the principle that tissue architecture explains the resilience of normal function in the face of mutations and other external perturbations[68]. Organized asymmetry is therefore an important basic feature of tissues; there must be distinctive topologies on which receptors assemble in order to correctly integrate the signaling patterns associated with tissue-specific functions. Tumor microenvironments should also possess combinatorial signaling asymmetries, though the microenvironments may be less obviously organized. One hypothesis is that the normal and tumor microenvironments integrate the signaling apparatuses differently, and thus therapeutic targets could be identified to selectively harm the tumor cells, and

microenvironment composition will be a determinant of drug efficacy. Those potential differences in signal integration can be revealed by technologies that recapitulate *in vivo* microenvironments, using defined physical, geometric, and molecular elements, and allowing one to assess the contribution of each property to emergent properties of tissues.

The complexity of microenvironments is a major impediment to understanding their impacts on cells. A majority of our understanding of biological mechanisms in human cells has been built upon the studies on two-dimensional plastic plates or dishes. Since the first human cell line, HeLa, was established on cell culture dishes, 2D cell culture has been a mainstay of biological research. However, as the dominant nature of the microenvironment over physiological processes has become increasingly appreciated, engineered 2D and 3D culture platforms that better recapitulate the molecular and physical nuances of the microenvironment *in vivo* are being developed.

It is an oversimplification to distinguish 2D and 3D culture platforms by dimensionality, the details of the culture microenvironments need to be considered and delineated with care to understand how each property effects cell physiology. Although 2D tissue culture plastic has been used extensively for biological research, they are far from physiological representations of tissues. In addition to the synthetic polymer composition of the plastic, cells in conventional 2D culture systems adhere to surfaces that are non-physiologically rigid (>2 GigaPascals Young's Elastic Modulus (GPa)) as opposed to the rigidity of normal tissue (Hundreds of Pa in soft tissues to tens of thousands of Pa for stiffer tissues

like cartilage and bone)[21, 69]. As the importance of microenvironment in therapeutic response has become more widely accepted, the urgency to identify tractable organotypic culture systems for studying human tissues *in vitro* has manifested.

Matrigel, HuBiogel, HuMatrix, and a number of other commercially available laminin-rich ECM are widely used to provide 3-D cell growth environments, and these gels are used increasingly to study the impact of drugs on cells grown in 3-D. Matrigel, which is harvested from a rodent sarcoma cell line, is comprised of hundreds of proteins that can vary significantly in the exact composition between production lots[70]. Recent adoptions of 3-D culture systems to high-throughput screening (HTS) systems are an important advance and use of 3-D gels in HTS studies is now a less daunting prospect, and achieving good quality imaging of cells in 3D seems to be the major rate-limiting step[71]. Biopolymers used for 3-D culture systems such as Matrigel are around 400Pa to 1kPa elastic modulus, and type I collagen gels can range from 500Pa to over 12kPa depending on collagen concentration. However, placing human cells in an undefined rodent sarcoma 3-D context may not mimic the intended *in vivo* microenvironment, and variability in the molecular components may confound interpretations and reproducibility of the results. Synthetic 3D culture hydrogels, such as polyethylene glycol based systems, offer precision tunability of the elastic modulus, which tends to cover a range similar to collagen gels, and allows control over molecular compositions[72].

Every *in vitro* system for studying tissue microenvironment sacrifices important aspects of the *in vivo* situation, but there is merit in studying

microenvironmental properties in isolation. Although engineered and biopolymer-derived systems necessarily over simplify tumor microenvironments, they can reveal important mechanistic elements of cellular responses by winnowing down the possible candidate pathways involved in a given functional response. The microenvironment can be dissected into biophysical (e.g. rigidity, shear force), biochemical (e.g. ECM, growth factors, cytokines), and architecture (e.g. dimension and geometry.), and each property plays a role in regulating cellular functions. For instance, by isolating and normal mammary epithelial cells in the context of matrix rigidity, in isolation from many other microenvironment properties, we discovered age-dependent regulation of the mechanotransducing YAP/TAZ transcription factors[73]. That we focused on mechanobiology from the outset made it possible to test hypotheses that revolved around pathways known to be involved in mechanobiology, and it revealed important information about age-related functional changes that also happen *in vivo*. Similarly, by using engineered polymer surfaces, we showed that substrate rigidity is a determinant HER2-targeted therapeutic efficacy via YAP/TAZ signaling pathway, both *in vitro* and *in vivo*[39]. While the microenvironments are deconstructed and different properties are studied individually or in defined combinations, the knowledge that we accrue over time allow us to form a portrait that models, and possibly explains, microenvironment affects on cellular functions.

1.7. Combinatorial microenvironment platforms mimic diverse and defined microenvironments and meet higher throughput ability.

Established human cell lines and primary cells propagated in 2D culture are

amenable to high-throughput experimentation. Potentially powerful tools for performing drug design in microenvironmental contexts are being developed by merging together the flexibility of functional cell-based screening with the highly parallel nature of microarray-type experiments. A microarray is a device that contains thousands of functionalized probes immobilized on a substrate. Microarray-type tools provide both complexity and high throughput ability, and are used to explore diversity in various biological systems. Broadly speaking the technology can be classified into protein arrays, gene chips, or carbohydrate microarrays, depending upon what probes are immobilized on the substrate[74]. An interesting innovation in this technology space has been to fabricate microarrays on 2D and 3D substrata, printing proteins that support adhesion of cultured cells. These types of combinatorial microenvironment microarrays (MEArrays) facilitate highly parallel cell-based functional screening. Indeed, Using different ECM and growth factor, pathway-blocking or –activating antibodies in various combinations as printed probes, enables molecular dissection of more complicated 3D microenvironments (Figure 22; reviewed in refs. [61-64, 72, 75].)

1.8. Summary.

In order to understand how microenvironment can modulate drug responses, we (LaBarge laboratory) has developed an MEArray platform in which combinatorial microenvironments can be controlled, and microenvironmental impact to cellular functions can be measured. My first work was to test the hypothesis that matrix rigidity is one of the determinants for lapatinib responses. Then I adapted and developed the MEArray with PA gels incorporated. Finally, I applied the MEArray

platform and demonstrated that MEArray is a feasible tool for testing our hypothesis that microenvironment is important to modulate therapeutic responses and needs to be considered in therapeutic designs.

Chapter 2: Materials and methods

2.1. Cell culture and drug treatment.

HCC1569 (American Type Culture Collection; Manassas, VA, USA) and BT549 breast cancer cell lines (gift from Dr. Joe W. Gray; Oregon Health & Science University, Portland, OR, USA) were maintained in RPMI1640 (invitrogen, Carlsbad, CA, USA) with 10% fetal bovine serum (FBS; Gemini Bio-Products, West Sacramento, CA, USA), and 1% Penicillin/Streptomycin/Glutamine (invitrogen, Carlsbad, CA, USA). Human mammary progenitor-derived cell line, D920 cells, at passage 63 were cultured in H14 medium on Vitrogen-coated (Cohesion) flasks for no more than 8 additional passages before starting from a fresh vial[62]. For drug treatment in 2D cultures, cells were cultured in 24-well plates with RPMI1640 with 1% FBS and 1% Penicillin/Streptomycin/Glutamine for 48 h after initial adhesion, and were then treated with lapatinib (1.5μM, LC Laboratories, Woburn, MA, USA) for an additional 48 h. For drug treatment in 3D cultures, cells were cultured in 24-well plates coated with Matrigel (BD Biosciences, San Jose, CA, USA) following the so called 'on top' protocol adapted from Lee, GY et al.[76], using a 5% Matrigel drip (cells were cultured on top on the drip of the Matrigel), then drugs or control were added on day 4 after cell plating for an additional 48 h. Other pharmaceutical and recombinant protein modulators were added concurrently with lapatinib: i.e. Verteporfin (VP, Sigma-Aldrich, St. Louis, MO, USA), was added at 0.2, 2, and 10 μg/mL; recombinant human amphiregulin (AREG, Sigma-Aldrich, St. Louis, MO, USA) at 5 ng/mL;

erlotinib at 1.5 μM; Blebbistatin (Bleb, Sigma-Aldrich, St. Louis, MO, USA) at 10 μM; and y27632 (Sigma-Aldrich, St. Louis, MO, USA) at 10 μM.

2.2. Tunable elastic modulus cell culture substrate fabrication.

Polyacryamide (PA) gels were polymerized on 12mm diameter coverslips etched with 0.1M NaOH, adapted from Tse, JR et al.[77]. 3% of acrylamide and 0.06% of bis-acrylamide were used to generate 400 (Elastic(Pascal) PA gels; 4% of acrylamide and 0.15% of bis-acrylamide were used to generate 2500 Pa PA gels. Sulfo-SANPAH (sulfosuccinimidyl 6-(4'-azido-2'-nitrophenylamino)hexanoate)(0.5 mM, ProteoChem, Loves Park, IL, USA) was added on PA gels and activated by UV light exposure for 10 min. PA gels were washed with HEPES buffer and then incubated with type 1 collagen (calf skin, Sigma-Aldrich, St. Louis, MO, USA) at RT for 2 h (0.1mg/mL in 50mM HEPES, Sigma-Aldrich, St. Louis, MO, USA). Gels were rinsed with copious amounts of PBS prior to placing them in 24-well plates treated with polyHEMA (0.133mL at 12mg/mL in 95% EtOH, Sigma-Aldrich, St. Louis, MO, USA) for cell culture.

2.3. Proliferation assay

5-ethynyl-2'-deoxyuridine (EdU) incorporation and staining were performed according to the manufacturer's protocol (invitrogen, Carlsbad, CA, USA). Nuclei were stained with Hoechst 33342. Images were captured with Zeiss 710 LSM (Carl Zeiss) confocal microscope, and images were segmented, and analyzed

with Image J (NIH) and CellProfiler, an open source image analysis software[78]. Drug response values are expressed as a relative incorporation of EdU, expressed as a percentage of EdU incorporation relative to control cells in DMSO only.

2.4. Transfection.

Cells were transfected with YAP, WWTR1 (TAZ), AREG, or non-silencing control siRNA (NSC) (SMARTpool: ON-TARGET plus, GE Dharmacon, Lafayette, CO, USA) with a FITC label (siGLO Green Transfection Indicator, GE Dharmacon, Lafayette, CO, USA), using DharmaFECT 2 Transfection Reagent (GE Dharmacon, Lafayette, CO, USA) according to the manufacturer's protocol, 72 h prior to assay performance.

2.5. Immunofluorescence staining.

Cells were fixed in 4% PFA (paraformaldehyde) at RT (room temperature) for 10 min; and for MEArray, cells were fixed in Methanol/Acetone (1:1) at -20 °C for 20 min. Cells were then blocked with PBS, 5% normal goat serum, and 0.1% Triton X-100 at RT for 30 min, then incubated with primary antibodies over night at 4°C. The primary antibodies I used were anti-YAP (1:100, Santa Cruz, Dallas, TX, USA), anti-TAZ (1:200, Cell Signaling Technology, Beverly, MA, USA), anti-HER2-alexa647 (1:100, Biolegend, San Diego, CA, USA), or anti-pHER2-1221/1222 (1:100, Cell Signaling Technology, Beverly, MA, USA). Primary antibodies were visualized with fluorescent secondary antibodies raised in goats (1:500, invitrogen, Carlsbad, CA, USA) together with Hoechst 33342 (1:200,

Sigma-Aldrich, St. Louis, MO, USA) incubated at RT for 2 h. Images were captured with a Zeiss 710 LSM confocal microscope (Carl Zeiss). Cell segmentation and single cell fluorescence intensities were analyzed with Matlab script adapted from[73] or CellProfiler[78]. For quantification of YAP/TAZ localization, the (N/C) ratios of mean fluorescence intensity in the (C)ytoplasmic and (N)uclear compartments of segmented cells were used. The cutoffs of $\log_2$ ratios were used to establish the three classes: C > N (X < -0.074), N = C (-0.074 < X < 0.074), and N > C (X > 0.074).

2.6. Real-Time PCR.

Total RNA was extracted with Trizol (invitrogen, Carlsbad, CA, USA) and purified by RNeasy prep (Qiagen, Valencia, CA, USA). cDNA was synthesized with SuperScript III RT (invitrogen, Carlsbad, CA, USA). Transcripts levels were measured by quantitative real-time PCR (qRT-PCR) with iTaq SYBR Green Supermix (BioRad Laboratories, Hercules, CA, USA) and Light Cycler480 (Roche, Indianapolis, IN, USA). Primers sequences were: YAP 5'-AGCCAGTTGCAGTTTTCAGG-3' and 5'-AGCAGCAATGGACAAGGAAG-3'; TAZ(WWTR1) 5'-GGAGAAAACGCAGGACAAAC-3' and 5'-TCATTGAAGAGGGGGATCAG-3'; AREG 5'-GTGGTGCTGTCGCTCTTGATA-3' and 5'-ACTCACAGGGGAAATCTCACT-3'; GAPDH 5'-AAGGTGAAGGTCGGAGTCAAC-3' and 5'-GGGGTCATTGATGGCAACAATA-3'.

2.7. Flow Cytometry.

Cells were collected via EDTA-PBS (0.4%EDTA) treatment without trypsin on ice. After washing with PBS, cells were blocked with PBS containing 2% bovine serum albumin, 5% normal goat serum, and 5mM EDTA, on ice for 30 min. Cells were incubated with the primary antibody anti-AREG (1:100, R&D Systems, Minneapolis, MN, USA) on ice for 30 min, washed with PBS, then treated with the secondary antibody on ice for 15 min. After 2 PBS washs, the level of AREG bound on cell membrane was measured with a FACSCalibur (Bekton-Dickenson).

2.8. AREG ELISA.

The intracellular AREG protein level was measured according to the manufacturer's protocol (Abcam, Cambridge, MA, USA), after 72 h in HCC1569 cells cultured on 2D TCP and 400 Pa PA gel with YAP knockdown by siRNA.

2.9. Animal experiment.

Six-week old female nu-/- mice were obtained from Taconic (Germantown, NY, USA) and housed five per cage with chow and water *ad libitum* in a controlled animal barrier. After 1 week, animals were injected s.c. into the upper flank with 3.5 to 5 million shRNA YAP HCC1569 cells. On Day 13 after tumor injection, when the average tumor volume was 150-200mm^3, IPTG and lapatinib treatment were administered for 2 weeks. IPTG (Sigma-Aldrich, St. Louis, MO, USA) was mixed into the drinking water at 10mM/1% glucose in light-protected bottles and changed every 2-3 days. Lapatinib was administered at 75 mg/kg/day body weight divided into twice daily dosing by oral gavage. Tumor dimensions (width,

height, and depth) were measured biweekly. At the time of sacrifice, animals were euthanized, and tumors were harvested and either immediately snap frozen or fixed in formalin. Animals were monitored for toxicity by measuring weight, assessing overall activity, and performing necropsy. All experimental procedures were followed according to the UCSF Animal Welfare Committee's approved policies and guidelines.

2.10. Human Phospho-Receptor Tyrosine Kinase (RTK) Array.

HCC1569 were cultured on 400 Pa and 40 kPa PA gel for 48 h, treated with lapatinib (1.5 μM) or DMSO, and then harvested at 1 h or 48 h after lapatinib treatment. The phosphorylations of 49 different RTKs were measured according to the manufacturer's protocol (Cat # ARY001B, Lot # 1323072, R&D Systems, Minneapolis, MN, USA).

2.11. Microenvironment microarray (MEArray).

The details of the MEArray preparation are described in our previous work[64]. The protocol includes the printing substrata preparation, protein master plate preparation, MEArray printing, and culturing cells on MEArray.

2.11.1. Printing substrate preparation.

For etching the slides, the slides were placed on heat block at 80°C, 1 mL NaOH was added on each slide, and allowed to evaporate completely. For providing cross-linkages between slides and PA gels, 250 μL of 3-Aminopropyltriethoxysilane (APES) was added on each slide for 5 min in the fume hood, slides were washed with H_2O thoroughly, and then slides were

placed in a 15 mL dish containing 25 mL of 0.5 % Glutaraldehyde in PBS for 30 min for activating the APES. 2500 Pa and 40 kPa polyacrylamide (PA) gels were prepared according to the recipe of the protocol and 350 µL of PA gel solution was applied on each slide. Let the gels polymerized for 90 min, wash the gel slides in H_2O at 4°C overnight, and then the gel slides were ready to be used for printing MEArray.

2.11.2. Protein master plate preparation.

Master plate for MEArray was prepared according to the protocol as Lin et al.[64]. Fibronectin (Sigma-Aldrich, St. Louis, MO, USA), type I collagen (Sigma-Aldrich, St. Louis, MO, USA), type IV collagen (EMD Millipore, Hayward, CA, USA), and laminin 1 (Sigma-Aldrich, St.Louis, MO, USA) were used as major ECM for supporting cell adhesion. Epidermal growth factor (EGF, Sigma-Aldrich, St. Louis, MO, USA), growth arrest-specific 6 (Gas6, R&D Systems, Minneapolis, MN, USA), interleukin 6 (IL6, Biolegend, San Diego, CA, USA), interleukin 8 (IL8, Biolegend, San Diego, CA, USA), amphiregulin (AREG, R&D Systems, Minneapolis, MN, USA), hepatocyte growth factor (HGF, R&D Systems, Minneapolis, MN, USA), and transforming growth factor beta (TGFB1, Biolegend, San Diego, CA, USA) were used combined with major ECM. Combinatorial microenvironments were prepared in 384-well plates in printing buffer (100 mM acetic acid, 20 % glycerol, 0.05 % Triton-X-100, pH3.8).

2.11.3. MEArray printing.

The quill pin printer, SpotBot III (Arrayit Corporation, Sunnyvale, CA, USA), was used for printing MEArray. In order to reach statistical power, 30 replicated spots

were printed for each combinatorial microenvironment on each slide. In total 1920 features were printed on each gel slide and spaced 350 μM apart.

2.11.4. Culturing cells on MEArray.

Gel slides with printed combinatorial microenvironments were placed in 4-well plates with PBS containing 1 % Penicillin/Streptomycin/Glutamine and 0.1 % Fungizone (Thermo Fisher, Waltham, MA, USA) for sterilization for 1 hr. The PBS was then replaced with complete medium, RPMI1640 supplemented with 10 % FBS and 1 % Penicillin/Streptomycin/Glutamine. For improving adhesion, the cells were added at a final concentration of 5 x 10^5 per well, 10^6 cells mL^{-1}, for 10 min, and then 4 mL complete medium was added for further adhesion for 2 hr. The unbound cells were then washed away with PBS.

2.11.5. Data analysis.

Images were thresholded, segmented, analyzed by CellProfiler[78]. The analysis of the fluorescence information and cellular morphological parameters were conducted in R[79]. The fluorescence intensity (488 nm) was determined for quantification of EdU incorporation ratio, and fluorescence intensities of pHER2 (568 nm) and HER2 (647 nm) were determined for assessing pHER2 and HER2 protein level. PCA and ViSNE analysis were performed for pattern clustering and dimension reduction[80, 81]. GLM analysis and the post-hoc analysis was performed in R package phia[82] to test the significance of lapatinib responses among various combinatorial microenvironments[72].

2.11.6. Validations of candidates.

The microenvironments that showed significant impact to lapatinib responses were validated on PA gel coverslips as previous described in materials and methods 2.2.

2.12. Statistics.

Significance was considered $p < 0.05$ or better using T-tests and Pearsons correlations. Those tests and area under the curve calculations were performed with Prism (Graphpad). * $p < 0.05$, ** $p < 0.01$, *** $p < 0.001$.

Chapter 3: Results

3.1. Microenvironment rigidity modulates responses to the HER2 receptor tyrosine kinase inhibitor lapatinib via YAP and TAZ transcription factors.

3.1.1. Rationale.

Microenvironment rigidity can promote tumor progression and survival through activation of growth factor signaling pathways, by enhancing integrin clustering and focal adhesion assembly[24, 25], or through modulation of microRNA expression[26]. For instance, the distinct drug responses have been observed between different culture microenvironment, 2D vs. 3D[23]. One of the obvious differences between 2D and 3D is the matrix rigidity, where the stiffness of plastic (2D) is more than 2 GPa and Matrigel (3D) is 400 Pa. Thus, I hypothesized that matrix rigidity is one of the major factor altering drug responses.

3.1.2. Summary.

I examined whether matrix rigidity impacted lapatinib responses in HER2-amplified breast cancer cells, using polyacrylamide (PA) hydrogel-based culture substrata that enabled control over the Young's elastic modulus (E[Pa]). The Hippo pathway mechanotransducers TAZ and YAP[83], which are also oncogenes [84], were required for the modulus-dependent responses *in vitro*, and downregulation of YAP *in vivo* slowed HER2-amplified tumor growth and improved sensitivity to lapatinib. YAP and TAZ did not mediate resistance by redundant activation of other HER family receptors. Our results suggest that rigid

microenvironments can modulate lapatinib resistance in HER2-amplified breast cancer cells via a YAP/TAZ-dependent mechanism.

3.1.3. Substrate elastic modulus is a modifier of lapatinib responses in HER2-amplified breast cancer cells.

To facilitate further investigation of microenvironment-directed drug responses, we identified a breast cancer cell line and pathway-targeted drug combination that offered a potentially wide dynamic range of response. Previous work demonstrated that the use of 2-D TCP versus 3-D Matrigel culture microenvironments modulated the anti-proliferative responses of four different HER2-targeted therapeutics that were used to treat four different HER2-amplified breast cancer cell lines. The combination of HCC1569 cells, a basal A subtype cell line[85], and lapatinib demonstrated the optimal differential response between TCP and 3-D[23]. First, our analysis methodology was validated by showing that HER2-amplified HCC1569 breast cancer cells conformed to previous findings, *i.e.* that they are more sensitive to the anti-proliferative effect of lapatinib in 3-D Matrigel compared to cells on 2-D TCP[23]. After plating on type 1 collagen-coated 2-D TCP or in 5% “ontop” 3-D Matrigel, cells were treated with DMSO or 1.5 μM lapatinib, a dose that was comparable to the average concentration in patient blood serum[86]. The magnitude of the anti-proliferative effect of lapatinib was determined by measuring 5-ethynyl-2’-deoxyuridine (EdU) incorporation into nuclear DNA, as a proxy for cell proliferation. Cells in 3-D were more sensitive to lapatinib compared to on TCP, with 21±2.6% and 69±9.7% EdU incorporation, respectively (Figure 1, A and B). Proliferation of the HER2-negative cell line

BT549 was not affected by lapatinib treatment (Figure 1, A and B). The differential anti-proliferative response between TCP and 3-D is partly explained by the distinct molecular compositions of the two culture microenvironments; indeed, it is already known that the increased sensitivity in 3-D is due partly to b1 integrin-mediated ECM adhesion[23]. However, there are other potential microenvironment characteristics that bear scrutiny in this drug response context.

One of the major differences between TCP and 3-D Matrigel is the rigidity of the culture substrata. Thus, the hypothesis that rigidity is a modulator of responses to lapatinib, in the HER2-amplified breast cancer cells was examined. The Young's elastic modulus (E[Pa]scals) of Matrigel has been estimated at 400 Pa[87], on a par with normal breast tissue[21]. In contrast, the elastic modulus of TCP is in excess of 2 GigaPa (GPa)[69, 88], which is well outside the physiological range[89]. To examine the role played by matrix rigidity in lapatinib responses, cell culture substrata were fabricated from PA gels, tuned to 400±160 Pa and coated with a type 1 collagen to support cell adhesion. HCC1569 were more sensitive to lapatinib on 400Pa PA gels compared to those on TCP coated with type 1 collagen, with 50±4.5% and 69±4.5% EdU incorporation, respectively (Figure 1, C and D); BT549 were not affected either by lapatinib or changes in rigidity (Figure 1, C and D). The half-maximal inhibitory concentration (IC50) of lapatinib was 3-fold lower on 400 Pa PA gels compared to TCP, 0.9 μM and 2.7 μM, respectively (Figure 1E). Thus, HCC1569 responded to lapatinib in an elastic modulus-dependent manner, showing greater resistance to the anti-proliferative effect of lapatinib on rigid matrices.

3.1.4. Actinomyosin network is involved in modulus-dependent lapatinib responses.

Cells sense the mechanical cues of microenvironment via mechanosensing-related pathways, such as Rho/ROCK signaling pathway, stretch activated channel, and force-induced protein unfolding[90]. To test the hypothesis that mechanosensing pathway plays a role in modulus-dependent lapatinib responses, I perturbed Rho/ROCK signaling pathway with inhibitors against different downstream factors in HCC1569 cells grown on 400 Pa gels, Matrigel, or TC dishes in the presence of lapatinib. Inhibitors of myosin II (Blebbistatin), and ROCK1/2 (Y27632) were used individually and together with lapatinib. These inhibitors eliminated modulus-dependent lapatinib resistance between TC dishes and 400 Pa gels (Figure 2, A and B). However, the inhibitors showed no significant effect between TC dishes and Matrigel, with lapatinib treatment (Figure 2, C and D). These results suggested that mechanosensing pathway, Rho/ROCK signaling pathway was involved in modulus-dependent lapatinib responses, but other molecular compositions in Matrigel also contributed to lapatinib responses. To identify the molecular compositions in Matrigel that modulate lapatinib responses, more studies, tools, such as MEArray, and proper statistical analysis are needed.

3.1.5. YAP and TAZ are required for the modulus-dependent lapatinib responses.

YAP and TAZ are Hippo pathway transcriptional co-activators that interact with the Rho/Rock pathway[83], and play an important role in transducing information

about substrate rigidity from the plasma membrane into the nucleus, where a transcriptional response is generated[35]. Consistent with their role in mechanotransduction, YAP and TAZ relocated from the cytoplasm into the nucleus as substrata stiffness increased (Figure 3, A and B). The effect of YAP and TAZ knockdown by siRNA on modulus-dependent responses to lapatinib was accessed. Both YAP and TAZ knockdown (Figure 6A) eliminated the modulus-dependent lapatinib resistance on TCP (Figure 3C). Disruption of the TEAD-YAP interaction with the 2 μg/mL of the inhibitor verteporfin[91] phenocopied the effect of YAP knockdown (Figure 3D). Indeed, increasing concentrations of verteporfin diminished the effect of modulus-dependent lapatinib resistance in a synergistic manner with lapatinib (Figure 7). YAP and TAZ were thus shown to be necessary for generating the modulus-dependent lapatinib resistance.

3.1.6. YAP knockdown *in vivo* increased sensitivity to lapatinib treatment.

To test whether YAP similarly played a role in lapatinib responses *in vivo*, we used Isopropyl β-D-1-thiogalactopyranoside (IPTG)-induced shRNA to knock down YAP in HCC1569 cells that were implanted in mice. Tumor volume was measured during the course of lapatinib treatment (Figure 4). Mice that neither received IPTG nor lapatinib (group A) had the maximum tumor volume (mean of volume, 1280 mm^3) by day 23. Mice treated with IPTG (group B) had significantly decreased ($p < 0.05$) tumor volume (mean of volume, 770 mm^3) compared to group A. Both lapatinib treatment groups, either with (group D) or without IPTG treatment (group C), had much smaller tumor volumes compared to groups A

and B. Group D, which received lapatinib and had reduced YAP levels, had the smallest tumor volumes (mean of volume, 192 mm^3), even compared to group C (mean of volume, 269 mm^3); however, that difference was not statistically significant. These data demonstrate that YAP knockdown was sufficient to reduce growth of HER2-amplified cell lines *in vivo*, and they suggest that YAP knockdown and lapatinib together may have some synergistic benefit. More comprehensive animal studies are required, however, to clarify the independent versus synergistic effects.

3.1.7. Modulus-dependent lapatinib responses are driven by multiple factors.

We sought to delineate other components of the molecular circuitry that enabled YAP to mediate the modulus-dependent response to lapatinib. Analysis of breast cancer data from The Cancer Genome Atlas data[3] showed that *YAP* mRNA expression correlated positively with expression of two known YAP targets *CTGF*, as well as with *AREG*[92], which is an EGFR ligand that has been attributed with multiple roles related to tumor invasion and drug resistance[93, 94](Figure 8). *HER2* (encoded by *ERBB2* gene) mRNA expression positively correlated with amphiregulin (*AREG*), inversely correlated with *EGFR* and *ERBB3* mRNA levels. Taken together, higher *AREG* expression correlated with *YAP* and *HER2* expression in breast cancers.

AREG, which has been shown to mediate EGFR-HER3 heterodimer formation and activate the ERK-Akt signaling pathway[95], and HER3-mediated PI3K/Akt activity was correlated with lapatinib resistance in HER2-amplified

breast cancer cells[96] was further examined. Paracrine AREG signaling in colorectal cancer cells also was shown to sustain ERK signaling and confer resistance to EGFR inhibitors[97].

AREG mRNA levels in HCC1569 cells showed a modestly increasing trend as the culture substrate rigidity was increased (Figure 5A), but cell membrane surface AREG protein level increased only about 4% (Figure 5B). To mimic the presence of a paracrine source of AREG, exogenous recombinant AREG (5 ng/mL) was added to cells, which caused increased nuclear YAP localization, even on compliant 400Pa surfaces (Figure 5C), and on compliant surfaces conferred lapatinib resistance to cells (Figure 5D). Simultaneous addition of exogenous AREG and the EGFR receptor inhibitor, erlotinib, reduced the resistance phenotype, demonstrating that exogenous AREG was exerting its effect partly through EGFR (Figure 5D). Knockdown of AREG by siRNA (siAREG) did not affect other ligands of EGFR, such as EGF or TGF-α, nor did it affect the receptors EGFR or HER2 (Figure 6B). YAP knockdown with siRNA decreased AREG expression 25%, suggesting that YAP modulates AREG (Figure 5E). These data together suggest that AREG is putatively involved in the modulus-dependent lapatinib responses. However, direct targeting of AREG via siAREG showed no significant effect on modulus-dependent lapatinib responses (Figure 5F). Because AREG was reported to cause activation of HER3[95], we examined modulus-dependent changes in HER3 phosphorylation, as well as from 49 other receptor tyrosine kinases, at 1 h and 48 h after attachment, Without lapatinib treatment, HER2 showed a higher phosphorylation on compliant substrata (400

Pa) within the first hour and increased phosphorylation after 48 h. However, consistent with the notion that AREG was not playing a significant role in modulus-dependent responses, HER3 was unchanged within the first hour and was decreased by 48 h (Figure 9). With lapatinib treatment, both HER2 and HER3 showed a decreased phosphorylation within 1 h, and then HER3 showed a subtle increased phosphorylation by 48 h on stiffer substrata (40 kPa). Taken all together, modulus-dependent lapatinib resistance cannot be explained from a single YAP-AREG circuit.

3.2. Fabrication and Use of MicroEnvironment microArrays (MEArrays).

3.2.1. Rationale.

Matrix rigidity, molecular composition, and architecture of microenvironment can contribute to modulate cellular functions individually, and the impact of interactions among these individual elements to cellular functions complicated the understanding of underlying mechanisms. A tool to deconstruct and control these microenvironmental properties is needed to access and quantify the functional studies and cellular phenotype as a function of defined microenvironment.

3.2.2. Summary.

We developed the microenvironment microarray (MEArray) platform for cell-based functional screening of interactions with combinatorial microenvironments[98]. The simultaneous manipulation of both the molecular composition and the matrix rigidity, combined with widely available microarray

and basic micropatterning technologies, allowed us to probe the impact of defined microenvironment to the cellular functions. MEArray screens require as few as 10,000 cells per array, which facilitates functional studies of rare cell types such as adult progenitor cells.

3.2.3. A flow chart of the MEArray procedure.

MEArrays can be printed using a wide variety of recombinant growth factors, cytokines, and purified ECM proteins, and combinations thereof. The platform is limited only by the availability of specific reagents. MEArrays are amenable to time-lapsed analysis, but most often are used for end point analyses of cellular functions that are measureable with fluorescent probes. For instance, DNA synthesis, apoptosis, acquisition of differentiated states, or production of specific gene products are commonly measured. Briefly, the basic flow of an MEArray experiment is to prepare slides coated with printing substrata and to prepare the master plate of proteins that are to be printed. Then the arrays are printed with a microarray robot, cells are allowed to attach, grow in culture, and then are chemically fixed upon reaching the experimental endpoint. Fluorescent or colorimetric assays, imaged with traditional microscopes or microarray scanners, are used to reveal relevant molecular and cellular phenotypes (Figure 10).

3.2.4. Verification of representative results.

An example of patterned protein deposition on a printed PDMS-coasted MEArray using a square-tipped silicon pins on a quill pin microarray-printing robot is shown in (Figure 11). Deposition of various proteins that are printed can be verified by immunofluorescence using antibodies (Figure 12). Dilutions of the

protein solutions in the master plate are reflective of the amount (fluorescent intensity) that is deposited on the printing substrata surface (Figure 12). Cells should attach to the printed features in an obvious patterned manner (Figure 13). An example of an MEArray experiment showing that inverse dilutions of two microenvironment proteins elicited specific keratin expression profiles in a protein concentration-dependent manner in a human multipotent mammary epithelial progenitor cell line (D920 cells), is shown in (Figure 14). Bubble plots are useful for determining whether specific phenotypes are imposed upon cells on replicate features of a dilution series. For instance, if a particular molecule in a microenvironment causes a distinct phenotype, once the instructive component has been diluted enough into a background of a neutral ECM the phenotype should change or disappear. Immunofluorescence detection of keratin 8 and keratin 14 intermediate filament proteins was performed with an Axon 4200a (Molecular Devices) microarray scanner. Twelve replicate dilution series were printed on each MEArray, and the $\log_2$ ratio of keratin 8 to keratin 14 mean fluorescence intensity was graphed as a bubble plot to give a realistic idea of variation and reproducibility of the signal. Shown is data from an MEArray that was fixed after cells had attached and unbound cells were washed away (Figure 14A), and after 24 hr of culture (Figure 14B). For this relatively small analysis, a one-way ANOVA was used to determine variance from the mean signal at each time point, and grouped two-tailed T-tests were used to determine whether the different dilutions of type I collagen and recombinant human P-cadherin caused changes in keratin expression. There was no variation from the mean among

cells on the features just after attachment; however, there were significant differences in keratin expression among cells after 24 hr of exposure to the different microenvironments. T-tests verified that high type I collagen concentrations elicited higher keratin 8 expression, whereas high P-cadherin concentrations elicited a strong keratin 14 signal after 24 hr. This result was consistent with previous reports that Pcadherin-containing microenvironments will impose of K14-expressing myoepithelial phenotype on bi-potent mammary progenitor cells[62]. An example of an entire scanned MEArray printed on a 40,000Pa PA gel is shown (Figure 15).

3.3. A continuum of therapeutic responses to a single pathway-targeted compound imposed by combinatorial microenvironments.

3.3.1. Rationale.

My first work showed that matrix rigidity is one of the important factors altering lapatinib responses. The results of mechanosensing perturbations with lapatinib suggested that not only matrix rigidity, but also the molecular composition in Matrigel could modulate lapatinib responses. We developed the MEArray for simultaneously investigating the impact of matrix rigidity and the molecular composition of microenvironment to drug responses. I applied the MEArray and asked the question that how matrix rigidity, molecular composition, and the interaction between these two microenvironmental properties modulate lapatinib responses.

3.3.2. Summary.

The results suggested that both matrix rigidity and the molecular composition alter lapatinib responses. Matrix rigidity conferred lapatinib resistance in HCC1569, which was consistent with our previous report[39]. The combined treatment of verteporfin and lapatinib has stronger inhibition to cells grown on softer substrate. I also identified candidates, such as fibronectin that may contribute to lapatinib resistance, for further validations and investigations of mechanisms.

3.3.3. Both molecular compositions and matrix rigidity alter morphological features.

With the MEArray, we were able to deconstruct and control both biophysical and biochemical properties of microenvironment to generate defined microenvironments and acquire multifaceted readouts of functional studies. The workflow of MEArray showed that even in a proof of concept experiment with low complexity of combinations of microenvironments, including four different major ECM compositions, seven recombinant proteins, two matrix rigidities, and three different drug treatments, it could yield more than two hundred defined microenvironments. The rich information in the output was single-cell resolution image data, including morphological features, the fluorescence intensity of targeted proteins, and functional measurements (Figure 16A). In order to reach better statistical power, we had 30 replicates for each defined microenvironment per slide, and 2 technique replicated slides for each MEArray experiment,

resulting in a total of 60 replicates for each condition. Each dot on slide was spaced by 350 μm to avoid direct contact between cells on every dot (Figure 16B). First, I asked whether cellular morphological features as well as cellular functions could be affected by matrix rigidity or molecular composition. The images were acquired by an epifluorescence microscope (Nikon), and the images were analyzed in Cellprofiler[99] to extract high-content information of measured features. To accommodate all information for visualization, cellular size and eccentricity, median intensity of HER2, and pHER2 staining were used in ViSNE to transform and project data into a scatter plot[81]. Each dot in ViSNE plot represented one defined molecular composition, and different color is either different matrix rigidity (Figure 16C) or different major ECM (Figure 16D). We showed that, dots were clustered based on matrix rigidity (Figure 16C) as well as major ECM component (Figure 16D), suggesting that both biophysical and biochemical properties of microenvironment impacted cellular features. The PCA analysis was performed to identify the major variants, and the microenvironmental components that contributed to alter these variants. Each dot represented one molecular composition, and colors represented matrix rigidities (Figure 16E) or different major ECM component (Figure 16F) in PCA analysis. The PCA analysis showed consistent conclusion with ViSNE that dots were clustered based on not only different matrix rigidity (Figure 16E) but also the molecular composition (Figure 16F). Furthermore, two major clusters, which were fibronectin and type IV collagen; and laminin I and type I collagen, were well separated either in ViSNE (Figure 16D) or PCA analysis (Figure 16F). In the

dimension one of PCA analysis, the major variants that were affected by microenvironments were number of neighbor cell and size of cell (Figure 17). Overall, we saw that the microenvironments influenced cellular morphological features.

3.3.4. Both molecular compositions and matrix rigidity impact lapatinib responses.

We then wanted to further investigate how microenvironment affected cellular function, such as lapatinib responses. Our previous report showed that lapatinib had a synergistic effect with verteporfin, that could eliminate modulus-dependent lapatinib resistance[39]. Thus, we studied the drug responses of cells that were cultured on either 2500 Pa or 40 kPa gels with either lapatinib alone or a combined treatment of lapatinib and verteporfin. In the ViSNE analysis, each dot represented one molecular composition, and different colors represented different drug treatments (Figure 18A), different major ECM components (Figure 18B), or drug sensitivity (Figure 18C). We first saw that cells on 2500 Pa with combined treatment were the most separated from other conditions (Figure 18A). Although the different drug treatments influenced clustering in ViSNE (Figure 18A), the clustering was still affected by the major ECM components, suggesting that major ECM component strongly influenced cellular features (Figure 18B). Interestingly, even though we did not use lapatinib sensitivity as a clustering factor in ViSNE, cells on 2500 Pa with combined treatment of lapatinib and verteporfin that showed the highest sensitivity, were distinctly separated solely based on morphological features (Figure 18C). After the z-score normalization

(normalized mean = 0, and positive and negative value indicates above and below the mean, respectively), the drug responses were quantified to relatively sensitive (blue color) or resistant (red color). Cells cultured on 40 kPa were generally more resistant to lapatinib, which is consistent with our previous report[39]. With the clustered heat map of z-score of EdU incorporation ratio normalized by DMSO control, the cells cultured on 2500 Pa with combined treatments showed the highest sensitivity (Figure 18D). The results also suggested that major ECM components influenced the lapatinib responses, e.g. cells on type IV collagen (red top legend) and on fibronectin (green top legend) were clustered closed, suggesting that these two ECM played important roles in altering drug responses (Figure 18D). The sub-group heat map showed that not only major ECM components, but also the interactions between ECM and other recombinant proteins, could modulate drug responses (Figure 18E). In conclusion, MEArray showed that matrix rigidity contributed to lapatinib resistance, and further showed that molecular compositions also influenced lapatinib responses.

3.3.5. A systematic analysis for impact of individual microenvironmental property as well as the pair-wise interactions of single property to lapatinib responses.

There were multilayers of factors involved in the *in vitro* cellular responses to drugs. In order to analyze the impact of individual components as well as pair-wise interactions between components, the general linear model (GLM) was applied to decouple the minor effects from the major one, and then quantify the

lapatinib responses as a function of microenvironment. Besides the major ECM proteins, such as fibronectin that conferred lapatinib resistance, other recombinant proteins showed various impacts as well, e.g. EGF was tended to increase the resistance of drug treatments, although these effects were minimal (Figure 19A). The combined treatment of lapatinib and verteporfin had a significant strong effect (Figure 19B), and the matrix rigidity conferred resistance to drug treatments (Figure 19D), which were consistent with our previous report[39]. Compared to type I collagen only, the combination of type I collagen and laminin I conferred higher cell sensitivity, and fibronectin conferred significant cellular resistance to lapatinib (Figure 19C). The synergistic or antagonistic effects of pair-wise interactions between components were also analyzed and presented (Figure 19E-H). Taken together, GLM analysis showed how each single microenvironmental component affected drug responses. Furthermore, several components, such as matrix rigidity or fibronectin, were found to correlate with lapatinib resistance.

3.3.6. The lower pHER2/HER2 status was correlated with higher lapatinib resistance.

Lapatinib inhibits proliferation via targeting HER2 receptors, thus, we hypothesized that the level of pHER2 and HER2, which could be affected by microenvironment, impacted lapatinib responses. I first asked whether the levels of pHER2 and HER2 were modulated by matrix rigidity. The pHER2 and HER2 level of HCC1569 cultured on type I collagen-coated gel with various matrix rigidities were measured by flow cytometry. The cells cultured on stiffer substrate

showed higher HER2 and lower pHER2 level (Figure 20A), suggesting a role of matrix rigidity in HER2 regulation. The pHER2/HER2 status was plotted against the lapatinib responses, and it showed that the higher lapatinib resistance of HCC1569 was correlated with lower pHER2/HER2 status (Figure 20B). With MEArray, I then asked whether molecular composition contributed to the pHER2/HER2 status and the lapatinib responses, and whether there were correlation between that and matrix rigidity. From all of the combinatorial microenvironments, the lapatinib resistance was trended higher (Figure 20C) and the pHER2/HER2 status was trended lower (Figure 20D) in HCC1569 cultured on stiffer substrate. However, the correlation between pHER2/HER2 status and lapatinib responses showed no statistical significance, suggesting that the molecular compositions may have various impacts on pHER2/HER2 and lapatinib response (Figure 20G). A waterfall plot of pHER2/HER2 status and lapatinib responses was presented with the same order of molecular compositions, and clearly showed that the lapatinib responses were not always inversely correlated with pHER2/HER2 status (Figure 20E-F).

3.3.7. Fibronectin conferred lapatinib resistance in HCC1569.

The microenvironments that showed prominent impact on lapatinib responses in HCC1569 were validated. Among all of the major ECM components, fibronectin conferred lapatinib resistance the most (Figure 19C). Fibronectin has been connected to breast cancer progression and tamoxifen resistance via the interaction with β1 integrin[100, 101]. Thus, the impact of adhesion to fibronectin was validated and showed that fibronectin conferred HCC1569 lapatinib resistance

(Figure 21A). We previously reported that lapatinib resistance is correlated with the activation of YAP. Thus the ratio of nuclear or cytoplasmic YAP localization in HCC1569 cultured on fibronectin-coated PA gels was quantified and showed that adhesion to fibronectin increased nuclear YAP localization (Figure 21B). To assess the impact of fibronectin on clinical outcome, analysis of breast cancer data from The Cancer Genome Atlas data (AgilentG4502A_07_3)[3] and The Cancer Proteome Atlas data (BRCA protein RBN)[102] were performed. The mRNA level of fibronectin was not correlated with mRNA of YAP, but the there was a positive correlation between fibronectin and YAP protein levels (Figure 21, C and D). Also, neither mRNA nor protein level of fibronectin were correlated with survival curve (Figure 21, E and F). Taken together, the results suggested that fibroenctin may contribute to lapatinib resistance via YAP-dependent pathways, but the mRNA and protein level of fibronectin were not directly correlated with clinical outcome.

Chapter 4: Discussion

4.1. The mechanosensing pathway and YAP are appealing therapeutic targets.

I first demonstrated that the mechanical property of microenvironments influenced resistance to and efficacy of the HER2 pathway-targeted therapeutic lapatinib, in HER2-amplified breast cancer cells. Although engineered culture substrata necessarily over-simplify the tumor microenvironment compared to *in vivo*, they can reveal important mechanistic elements of cellular responses, by winnowing down the possible candidate pathways that are involved in a given response. I specifically probed the property of elastic modulus on cells at low density on PA gels, to minimize the confounding effects of cell-cell contact. YAP activation is known to be regulated also by cell-cell contact[33], where high cell density inhibits YAP activation by inducing YAP phosphorylation. In our engineered system YAP and TAZ activation were correlated with resistance to lapatinib, and when YAP was knocked out in orthotopically-implanted tumors grown in mice, tumor growth slowed and they became more sensitive to lapatinib. The resistance phenotype is not exclusively modulus-dependent, but by isolating and studying that one physical property of the matrix, we revealed that the Hippo pathway is likely an important component of resistance in HER2-targeted kinase inhibitors.

YAP has been attributed with dual roles in tumorgenesis in breast cancer. Studies *in vitro* have shown that exogenous expression of YAP in cells can

promote cell growth, suggesting YAP has a role as a tumor promoter[84]. Others have reported potentially tumor suppressive roles for YAP. Loss of heterozygosity at the YAP locus in a number of luminal breast cancers, and shRNA knockdown of YAP in some breast cancer cell lines suppresses anoikis, which is a form of programmed cell death, and promotes tumor growth *in vivo*[103]. Moreover, YAP expression was reduced in some invasive carcinoma samples compared to normal breast tissues[104]. The multiple roles of YAP in tumorigenesis may be dependent upon the stage of a given cell's progression, e.g. active YAP enhances tumor growth when expressed in mammary carcinomas, but not when expressed in a non-malignant mammary epithelial cell line[105]. YAP expression in breast cancers may be subtype-dependent[106], and YAP is notably present in stromal cells[107], not only epithelial, which further complicates the *in vivo* situation. In addition, YAP and TAZ exhibit distinct functions, e.g. YAP knockout mice are embryonic lethal[108], but TAZ knockout mice can be viable although the animals have kidney disease [109]. Here we showed that either YAP or TAZ knockdown *in vitro* can eliminate modulus-dependent lapatinib responses and confer more sensitivity to lapatinib, suggesting redundant roles in the context of modulus-dependent response to lapatinib.

The photosensitizer, verteporfin (Visudyne®, Novartis), is used as photodynamic therapy for neovascular lesions in the eye[110]. In the absence of photoactivation, verteporfin can disrupt TEAD(Transcriptional enhancer factor TEF-1)-YAP association and inhibit YAP-induced liver overgrowth[91], suggesting a pharmacological strategy for regulating the transcriptional activities of YAP,

which requires TEAD family proteins to bind to DNA. While verteporfin is a well characterized, FDA approved drug for photodynamic therapy, the anti-tumorigenic effect of YAP-related mechanism in breast cancer has not been well studied. Our data show that verteporfin has a synergistic effect with lapatinib i*n vitro*, indicating that there is a potential benefit to testing the verteporfin in the context of lapatinib resistance.

Many studies into resistance to HER2-targeted cancer therapeutics have focused on intrinsic cellular mechanisms, such as compensatory pathway activation, but the tumor microenvironment will likely play an important role as well. Indeed, greater matrix rigidity leads to increased resistance to the anti-proliferative effects of lapatinib, in HER2-amplified breast cancer cells on culture substrata engineered to mimic different levels of matrix rigidity. Several studies have shown in various cancer contexts that increasing matrix stiffness can both promote chemotherapeutic resistance[27, 111, 112], and decrease sensitivity to Raf kinase inhibitors[113]; however, the mechanisms underlying these elastic modulus-dependent effects are not yet well defined.

Lapatinib resistance also has been linked to compensatory activation of HER3[14], but we did not find that HER3 was strongly activated in the context of increased matrix rigidity. To mimic levels found in patient serum, we used 1.5 μM lapatinib, a concentration considered high[14], and we measured HER3 phosphorylation 48 hours after lapatinib treatment, whereas compensatory activation of HER3 may occur after 72 hours and at a lower lapatinib concentration. Taken together, and experimental differences notwithstanding,

these reports suggest that resistance to HER2-targeted kinase inhibitors is likely a multi-faceted challenge still to be overcome.

4.2. Applications of MEArrays.

That most failures in drug development are due to a lack of efficacy suggests that our pre-clinical development toolbox does a poor job of predicting compound activity *in vivo*[114]. Multi-well TCP plates are still the substrate of choice for much of modern drug screening, which ignores an obvious lack of context[115]. Some high-throughput (HT) compatible 3-D culture systems are being developed to overcome this problem, but retooling of HT systems and improvements in image analysis algorithms remain significant barriers to wide-scale adoption. Adaptation of 2-D hydrogels that are controlled for tissue-like elastic moduli and are conjugated with tissue-like molecular milieus to HT systems might present an intermediate step that can both take advantage of existing HT systems and recapitulate some key elements of *in vivo* microenvironments that are crucial for determinants of drug responses.

MEArrays are enabling high-throughput functional exploration of stem cell niches. While these array platforms create caricatures of *in vivo* microenvironments, they enable researchers to functionally define molecular components that maintain adult and embryonic stem cells, thus revealing molecular regulators and pathways of the stem cell state. We predict this type of functional cell-based dissection of combinatorial microenvironments will have particular high impact in understanding normal and malignant human stem cells, because *in vivo* experiments are essentially impossible. For instance, putative

niche proteins and other tissue-specific proteins have been identified using MEArrays, and validated *in vivo* in some cases, that were relevant to human embryonic[61, 116], neural[63], mammary[62, 64], and hepatic stem cells[75]. MEArrays also were used to profile cell–ECM adhesion biases[117],and to optimize growth conditions of cultured cells[118]. Taking a combinatorial approach, relative to a candidate-based approach, allows screening combinations of multiple tissue-specific microenvironment proteins to identify extracellular cues that are the basis for emergent cell behaviors. Functional roles for a number of molecules known to be expressed in human mammary gland and brain, but hitherto had not been ascribed respective roles for mammary or neural stem and progenitor cell regulation, were discovered using this type of approach. The successful application of MEArrays requires managing a number of technical details that are, in many cases, on edge of discovery themselves. The remainder of this chapter will elaborate on some of the issues that arise most often when producing MEArrays on 2-D substrates and provide some discussion of how we are managing them. There are relatively fewer examples of MEArray-type platforms in 3-D, perhaps because some of the high-throughput liquid handling and 3-D imaging requirements raise the barrier to entry, however an excellent example of 3-D MEArrays is available in Ranga et al.[72].

4.3. Selecting the printing substrate: It depends on the biological questions being asked.

There are numerous materials used to immobilize proteins, but the main object remains the same where MEArray fabrication is concerned: a suitable surface

coating for printing proteins upon should provide high adsorption capacity, low cell attachment in areas not printed with proteins (i.e. non-fouling), and low spot-to-spot variation. Other important considerations for protein arrays include, the capacity to retain protein structure, functionality, and binding sites.

The most commonly used approaches are to chemically modify surfaces of glass slides, e.g. with aldehydes or epoxies, or to coat them with very thin layers of polymers such as polydimethylsiloxane (PDMS). Slides with these surfaces adsorb proteins with either covalent bonds or strong electrostatic interactions, respectively. Covalent modifications provide irreversible attachment, however protein 3-dimensional structures may not be well maintained. Unintended cell attachment also can be problematic with the chemically modified glass and with the hydrophobic PDMS without the addition of non-fouling coatings, like Pluronics F108 or bovine serum albumin. Another option is to coat glass surfaces with polyacrylamide (PA), or poly(ethylene glycol) (PEG) hydrogels. These types of hydrogels physically absorb proteins through relatively weak electrostatic interactions. This retains most of the native protein conformation, but there is higher variation in protein binding capacity[119]. One of the most convenient properties of PA and PEG gels is their native non-fouling character, which removes any problems of non-specific cell attachment.

Another important property to consider is the rigidity of the substrate. PDMS is inexpensive and it is easy to manipulate its elastic modulus by altering the cure:polymer ratio, and cover a range of rigidity similar to that of cartilage, skin, and tendon (0.6 to 3.5 MPa). PEG is commonly used in cell fate decision

studies, representing a range of rigidity from 500 kPa to 1.6 GPa. PA is another inexpensive substrate, which can be tuned from 150 Pa to 150 kPa, which is closer to the biological microenvironment for soft tissues like brain and breast[120]. Which substrate for protein immobilization should be used really depends upon the characteristics of cells used, the tissue structure being mimicked, and the outcomes being measured.

4.4. MEArray data analysis: Seeing the forest for the trees.

A main goal of MEArray-type experiments is to provide causal links between cellular responses and specific microenvironments. Both inter- and intra-microenvironment heterogeneity of cellular responses are to be expected, and can be instructive about the continuum of phenotypic plasticity within the experimental system. Measuring heterogeneity of drug responses in various contexts may result in more realistic expectations of drug responses *in vivo*. By incorporating sufficient numbers of replicate features into the design of a given MEArray, significant associations between microenvironments and cell phenotypes can be identified, but the high dimensionality of the data is a hindrance to extraction of meaningful information. Most MEArray platforms use fluorescent probes to visualize biochemical and functional phenotypes, and fluorescent and phase microscopy to capture morphological and colorimetric phenotypes. There are no specialized high-throughput imaging systems for this type of work currently available, however, microarray scanners, and programmable, motorized epifluorescence or laser scanning confocal microscopes have been successfully used to acquire the necessary images[62, 72].

Micrographs of cells attached to the various arrayed microenvironments can be treated as ensemble data, i.e. averaging the signal from many cells on one spot in a manner similar to DNA arrays, or as single-cell data when used in combination with cell segmentation algorithms. Even in cases where MEArrays are designed to have fairly low complexity, e.g. 100 or fewer unique microenvironment combinations, the analytical challenges are significant. The complexity of the information space generated from MEArray experiments increases rapidly when taking into consideration multiple microenvironmental properties such as rigidity, geometry, and molecular composition. In practice, the statistical analysis of MEArray experiments is a rate-limiting step for this technology, and there are multiple solutions for addressing this challenge. The basic data processing workflow for MEArray experiments includes: signal normalization, identifying functionally similar microenvironments by clustering, dimension reduction, data visualization, and further pathway analysis. Table 1 shows some suggested software packages that aid with analyses of MEArray-type data, with comments on specific strengths and weaknesses.

4.4.1. Data normalization.

All microarray-like data contain some useful information and a lot of noise, thus proper data normalization is crucial. The data analysis starts from measuring fluorescence intensity or colorimetric density of each target protein in cells on each array feature, where intensity reflects the relative abundance of the target protein. Intensities are impacted by factors, such as the characteristics of dye (antibody), spatial location, and uneven surfaces of the slides that cause

inconsistent background [121]. Unlike DNA microarrays, which load the same amount of cDNA onto the array and then uses total intensity as an internal reference, the number of cells attached on the MEArray features varies by microenvironment. Thus, we may use the average of the total signal from all cells on all array features as a reference for normalization of arrays of the same treatment condition. A signal emanating from cells on a control microenvironment, which is known *a priori* to reproducibly bias towards a given phenotype, can be used as a reference[62]. An alternative is to use spots that contain the same amount of fluorescence molecules and should have the same intensity as an internal control printed on each array. After proper normalization, the data are ready to be further analyzed.

4.4.2. Statistical considerations.

The main purpose of MEArray experiments is to identify the specific microenvironments that modulate certain cellular functions by comparing cellular phenotypes between treatments and controls. Table 2 shows some methods, which have been used for processing microarray data. Although Student's t-test is a widely used statistical test in biological research, it is valid only for comparing two sets of data with each other. Dunnett's t-test is the correct test for comparing multiple sets of data with a single control, and in this research for identifying multiple microenvironments that impose phenotypes significantly different from the control[62]. The Z-score standardization is a simple method used to identify meaningful groups that are distinct from the global mean. Z-scores were used successfully to identify and optimize better culture conditions for rare cell

populations[122]. However, Z-score has several limitations, like skewing of values due to outliers within a dataset, less accuracy when cell numbers are reduced, and the Z-score is based on the assumption that data fit a Gaussian distribution, which is not the case in many biological systems. Thus, Guyon et al. proposed the Φ-score as a cell-to-cell phenotypic scoring method for selecting the hit discovery in cell-based assays. The Φ-score ranks cells instead of averaging them, and shows performance that surpasses the Z-score for coping with the above limitations. Indeed the Φ-score can be more sensitive (more true hits) and more specific (fewer false positives) compared to other conventional methods[123].

Clustering methods commonly used for DNA microarray datasets, such as hierarchical or k-means clustering, also are used with MEArray data to separate meaningful groups. Konagaya et al. interrogated a relatively small number of growth factor combinations to optimize neural progenitor cell culture microenvironments, and they used hierarchical cluster analysis to reveal three major clusters of microenvironment combinations that facilitated growth versus astrocyte or neuron differentiation[124]. Although these analyses can reveal the meaningful groups within simple datasets, like traditional two-color DNA microarray data, the difficulty and challenge of data clustering arises rapidly in high dimensional data[125]. The phrase, “the curse of dimensionality”[126], described the general phenomenon that data analysis techniques ,which work well at lower dimensions, are often unable to perform well when the dimensionality of data are increased. Dimension reduction techniques have been developed to overcome some of these difficulties.

4.4.3. Dimension reduction and data visualization.

Thanks to improvements in computational processing power, we now are able to deal with high-dimensional data more easily and with algorithms that do not make painful compromises in the name of efficiency. The methods used for dimension reduction distill the information from a sea of data into snap shots that are emblematic of the underlying biology.

Principle component analysis (PCA) is used for dimension reduction and can reveal the most variable factors that contribute to certain phenotypes[127]. However, not all biological questions are related to the variables with highest variance in the dataset, and in these cases, PCA is less able to identify the contributing factors. Thus, Independent component analysis (ICA) is an alternative to PCA, particularly when we know some certain characteristics of our data, and assume that the observed data are separated into groups that are independent of each other[128]. An example of a case where ICA has been applied is the cocktail party problem, describing the human ability to selectively recognize speech sound which are often assumed to be independent from each other in noisy environment[129]. However, the need to make assumptions about the data and to choose the number of components analyzed is a limitation of ICA, particularly in high dimensional data sets where we may not fully understand the relationships between variables. Due to this limitation, Yao et al. proposed Independent Principle Component Analysis (IPCA) combining the advantages of PCA and ICA, where they applied PCA as a pre-processing step to extract components for subsequent analysis, and then applied ICA to filter out noise.

They assumed that microarray-based gene expression measurements that follow a Gaussian distribution represent noise (i.e. most of the genes are not expected to change at a given condition), and they showed that IPCA was better at revealing patterns in those biological data[130]. All of these approaches are used in microarray analysis, but they often suffer from preserving important information during data reconstruction when trying to analyze high dimensional single cell data. Linear techniques such as PCA focus on separating dissimilar data points far away in low-dimensional representations after data transformation. However, biological data is often non-linear, and for high dimensional data it is usually more important to keep similar data points close together in low-dimensional representations, which is typically not feasible with linear mapping techniques[131]. MEArray data are of a similar level of dimensionality to the data generated by techniques like Mass cytometry (CyTOF). CyTOF is being developed as a new single cell analysis technique that combines flow cytometry and transition element isotope labeling, and CyTOF allows one to simultaneously measure up to 100 protein markers inside and on the plasma membranes of cells[132]. CyTOF and MEArray experiments generate very high content information, incorporating information about multiple protein expression levels, multiple cellular morphology parameters, and other image-based measurements among different treatments, all at the single cell level. Qiu et al. developed and applied spanning-tree progression analysis of density-normalized events (SPADE) to mass cytometry data and demonstrated the ability of SPADE to recapitulate patterns of hematopoiesis and to identify subpopulations of cells[133]. Based on the t-SNE

technique, Amir et al. developed a non-linear approach called viSNE, for high-dimensional data visualization. They were able to identify a rare leukemia population when comparing leukemia diagnosis and relapse samples[81]. These latter two approaches take into account major and the minor sources of variance within a data and represent them on a low dimensional surface, which facilitates the visualization of high dimensional data. Once the meaningful information has been extracted, the data collected from MEArrays needs to be connected to the existing body of knowledge in order to perform further biological validation.

4.5. ECM proteins have major impact on lapatinib responses.

We previously showed that the matrix rigidity plays an important role in altering lapatinib resistance in HCC1569 via YAP-dependent mechanosensing mechanisms. However, the impacts of molecular compositions of Matrigel to lapatinib responses have not been well elucidated, yet. The reconstituted basement membrane (BM), Matrigel, is rich in laminin and collagen IV, and the signals from the BM regulate epithelial cellular functions in mammary cells[134, 135]. Although adhesion to type I collagen or laminin I conferred cells similar lapatinib responses (Figure 19C), the adhesion to both (1:1) showed higher lapatinib sensitivity, suggesting that the impact of interactions between molecular compositions could be different from impact of individual composition. Thus, the details of mechanisms about how molecular compositions altered lapatinib sensitivity required the consideration of context and more investigations for elucidation.

Recently, it has been shown that adhesion of cells to fibronectin activates FAK-Src-YAP pathway, suggesting a plausible linkage between fibronectin and YAP dependent pathway[136]. My results showed that fibronectin increased lapatinib resistance and nuclear YAP translocation (Figure 21, A and B), and it is likely that this fibronectin-induced nuclear YAP translocation contributed to lapatinib resistance via FAK-Scr-YAP pathway. The first step to test this hypothesis is to see whether the perturbation of FAK-Scr-YAP pathway can eliminate fibronectin-induced lapatinib resistance as well as nuclear YAP translocation. The expression of intracellular fibronectin has been connected to breast cancer metastasis and provides prognostic significances[137] and may account for chemotherapeutic resistance[101]. Thus, a comprehensive understanding of how fibronectin modulates drug responses is important for designing therapeutic strategies.

4.6. The effects from other recombinant proteins.

Unlike the major ECM, which had more prominent and consistent impact on lapatinib responses, the effects from recombinant proteins were much less (Figure 19A). One explanation is that the impacts from ECM were more dominant than recombinant proteins. Another explanation, which may also reflect the importance of microenvironments, is that the impacts from recombinant proteins to lapatinib responses are context-dependent and less consistent. For instance, the combination of HGF and fibronectin conferred the highest lapatinib resistance in 2500 Pa rigidity, but it showed minor impact on lapatinib responses in 40 kPa (Figure 18E). The individual effect of each recombinant protein was computed by

GLM analysis, which generated the adjusted lapatinib responses based on entire data set. Thus, the various lapatinib responses among total combinatorial microenvironments averaged out the impact of single recombinant protein.

In the MEArray experiments, cells were not only attached to the combinatorial microenvironments that were printed, but also exposed to the trace soluble components that were secreted by cells. It is likely that ECM, which cells attached to, could modulate the secretion of soluble factors that impacted cells. Although the impacts of these secreted components should not be ignored, we may argue that these secretions may be trivial compared to combinatorial microenvironments that cells directly adhered to. The volume of media that was used for cell culture might dilute these soluble factors significantly to minimize the impacts. Also, all cells in MEArray were exposed to a mixture of these diffused soluble factors, which should no longer have microenvironment-dependent impact. However, in order to really isolate and measure the impact of microenvironment-dependent secreted soluble factors, multiple-well plates might be used as an approach. For instance, if capable, the same replicates of combinatorial ECM can be printed in isolated wells of a 384 multiple-well plate, and the recombinant proteins added into wells one at a time. Thus, each well will contain only replicates of one defined microenvironment, and the cells will be exposed to the same microenvironment.

Chapter 5: Conclusions

5.1. Conclusions

The success rate of translation from pre-clinical drug screening to clinical efficacy is low, and it is also true in animal models, which serve as important sources *in vivo*[138]. Besides the intrinsic genetic alterations, and inter-patient variability and intra-tumor heterogeneity that modulate drug efficacy, emerging studies demonstrated microenvironment is also an important determinant that modulates therapeutic responses [139].

In summary, my research has demonstrated that the microenvironment has significant impact on responses of targeted therapy. Although this MEArray platform is not yet the model that can recapitulate real microenvironment *in vivo*, the information acquired by accessing the impact of combinatorial microenvironments can shed light on mechanisms of microenvironment-dependent drug responses. I showed that merely changing matrix rigidity alone could modulate lapatinib responses via YAP-dependent signaling pathway. The combinatorial microenvironments microarray (MEArray) we developed provides a feasible tool for answering questions such as how defined microenvironments impact cellular biology. With MEArray, I demonstrated that both matrix rigidity and molecular compositions could modulate lapatinib responses, and identified microenvironments, such as higher matrix rigidity or fibronectin, conferred lapatinib resistance. Further studies are needed and already in progress to

elucidate the mechanisms to overcome the microenvironment-induced lapatinib resistance.

Chapter 6: Reference:

1. Siegel, R.L., Miller, K.D. & Jemal, A. Cancer statistics, 2016. *CA: a cancer journal for clinicians* **66**, 7-30 (2016).
2. Society, A.C. Cancer Facts & Figures 2016. *Atlanta: American Cancer Society* (2016).
3. Koboldt, D.C. et al. Comprehensive molecular portraits of human breast tumours. *Nature* **490**, 61-70 (2012).
4. Nio, Y. et al. Anticancer chemosensitivity changes between the original and recurrent tumors after successful chemotherapy selected according to the sensitivity assay. *Annals of surgery* **221**, 89-99 (1995).
5. Kunz-Schughart, L.A., Freyer, J.P., Hofstaedter, F. & Ebner, R. The use of 3-D cultures for high-throughput screening: the multicellular spheroid model. *J Biomol Screen* **9**, 273-285 (2004).
6. Bissell, M.J., Radisky, D.C., Rizki, A., Weaver, V.M. & Petersen, O.W. The organizing principle: microenvironmental influences in the normal and malignant breast. *Differentiation* **70**, 537-546 (2002).
7. Kun, Y. et al. Classifying the estrogen receptor status of breast cancers by expression profiles reveals a poor prognosis subpopulation exhibiting high expression of the ERBB2 receptor. *Human molecular genetics* **12**, 3245-3258 (2003).
8. Kim, M., Agarwal, S. & Tripathy, D. Updates on the treatment of human epidermal growth factor receptor type 2-positive breast cancer. *Current opinion in obstetrics & gynecology* (2013).
9. Rexer, B.N. & Arteaga, C.L. Intrinsic and acquired resistance to HER2-targeted therapies in HER2 gene-amplified breast cancer: mechanisms and clinical implications. *Critical reviews in oncogenesis* **17**, 1-16 (2012).
10. Maximiano, S., Magalhaes, P., Guerreiro, M.P. & Morgado, M. Trastuzumab in the Treatment of Breast Cancer. *BioDrugs : clinical immunotherapeutics, biopharmaceuticals and gene therapy* (2016).
11. Lavaud, P. & Andre, F. Strategies to overcome trastuzumab resistance in HER2-overexpressing breast cancers: focus on new data from clinical trials. *BMC Medicine* **12**, 1-10 (2014).
12. Medina, P.J. & Goodin, S. Lapatinib: a dual inhibitor of human epidermal growth factor receptor tyrosine kinases. *Clin Ther* **30**, 1426-1447 (2008).
13. Rusnak, D.W. et al. Assessment of epidermal growth factor receptor (EGFR, ErbB1) and HER2 (ErbB2) protein expression levels and response to lapatinib (Tykerb, GW572016) in an expanded panel of human normal and tumour cell lines. *Cell proliferation* **40**, 580-594 (2007).
14. Amin, D.N. et al. Resiliency and vulnerability in the HER2-HER3 tumorigenic driver. *Science translational medicine* **2**, 16ra17 (2010).
15. Xia, W. et al. An heregulin-EGFR-HER3 autocrine signaling axis can mediate acquired lapatinib resistance in HER2+ breast cancer models. *Breast cancer research : BCR* **15** (2013).

16. Liu, L. et al. Novel mechanism of lapatinib resistance in HER2-positive breast tumor cells: activation of AXL. *Cancer research* **69**, 6871-6878 (2009).
17. Chen, C.T. et al. MET activation mediates resistance to lapatinib inhibition of HER2-amplified gastric cancer cells. *Molecular cancer therapeutics* **11**, 660-669 (2012).
18. Provenzano, P.P., Inman, D.R., Eliceiri, K.W. & Keely, P.J. Matrix density-induced mechanoregulation of breast cell phenotype, signaling and gene expression through a FAK-ERK linkage. *Oncogene* **28**, 4326-4343 (2009).
19. Engler, A.J., Sen, S., Sweeney, H.L. & Discher, D.E. Matrix elasticity directs stem cell lineage specification. *Cell* **126**, 677-689 (2006).
20. Provenzano, P.P. & Keely, P.J. Mechanical signaling through the cytoskeleton regulates cell proliferation by coordinated focal adhesion and Rho GTPase signaling. *Journal of cell science* **124**, 1195-1205 (2011).
21. Paszek, M.J. et al. Tensional homeostasis and the malignant phenotype. *Cancer Cell* **8**, 241-254 (2005).
22. Weaver, V.M. et al. beta4 integrin-dependent formation of polarized three-dimensional architecture confers resistance to apoptosis in normal and malignant mammary epithelium. *Cancer Cell* **2**, 205-216 (2002).
23. Weigelt, B., Lo, A.T., Park, C.C., Gray, J.W. & Bissell, M.J. HER2 signaling pathway activation and response of breast cancer cells to HER2-targeting agents is dependent strongly on the 3D microenvironment. *Breast cancer research and treatment* **122**, 35-43 (2010).
24. Rubashkin, M.G. et al. Force engages vinculin and promotes tumor progression by enhancing PI3K activation of phosphatidylinositol (3,4,5)-triphosphate. *Cancer research* **74**, 4597-4611 (2014).
25. Paszek, M.J. et al. The cancer glycocalyx mechanically primes integrin-mediated growth and survival. *Nature* **511**, 319-325 (2014).
26. Mouw, J.K. et al. Tissue mechanics modulate microRNA-dependent PTEN expression to regulate malignant progression. *Nature medicine* **20**, 360-367 (2014).
27. Schrader, J. et al. Matrix stiffness modulates proliferation, chemotherapeutic response, and dormancy in hepatocellular carcinoma cells. *Hepatology* **53**, 1192-1205 (2011).
28. Justice, R.W., Zilian, O., Woods, D.F., Noll, M. & Bryant, P.J. The Drosophila tumor suppressor gene warts encodes a homolog of human myotonic dystrophy kinase and is required for the control of cell shape and proliferation. *Genes & development* **9**, 534-546 (1995).
29. Zhao, B., Lei, Q.-Y. & Guan, K.-L. The Hippo–YAP pathway: new connections between regulation of organ size and cancer. *Current opinion in cell biology* **20**, 638-646 (2008).
30. Tapon, N. et al. salvador Promotes Both Cell Cycle Exit and Apoptosis in Drosophila and Is Mutated in Human Cancer Cell Lines. *Cell* **110**, 467-478 (2002).
31. Harvey, K.F., Zhang, X. & Thomas, D.M. The Hippo pathway and human cancer. *Nat Rev Cancer* **13**, 246-257 (2013).

32. Curto, M. & McClatchey, A.I. Nf2/Merlin: a coordinator of receptor signalling and intercellular contact. *British journal of cancer* **98**, 256-262 (2008).
33. Zhao, B. et al. Inactivation of YAP oncoprotein by the Hippo pathway is involved in cell contact inhibition and tissue growth control. *Genes & development* **21**, 2747-2761 (2007).
34. Mo, J.-S. et al. Cellular energy stress induces AMPK-mediated regulation of YAP and the Hippo pathway. *Nature cell biology* **17**, 500-510 (2015).
35. Dupont, S. et al. Role of YAP/TAZ in mechanotransduction. *Nature* **474**, 179-183 (2011).
36. Yu, F.X. & Guan, K.L. The Hippo pathway: regulators and regulations. *Genes & development* **27**, 355-371 (2013).
37. Acerbi, I. et al. Human breast cancer invasion and aggression correlates with ECM stiffening and immune cell infiltration. *Integrative biology : quantitative biosciences from nano to macro* **7**, 1120-1134 (2015).
38. Moroishi, T., Hansen, C.G. & Guan, K.-L. The emerging roles of YAP and TAZ in cancer. *Nat Rev Cancer* **15**, 73-79 (2015).
39. Lin, C.H. et al. Microenvironment rigidity modulates responses to the HER2 receptor tyrosine kinase inhibitor lapatinib via YAP and TAZ transcription factors. *Molecular biology of the cell* **26**, 3946-3953 (2015).
40. Johnson, R. & Halder, G. The two faces of Hippo: targeting the Hippo pathway for regenerative medicine and cancer treatment. *Nature reviews. Drug discovery* **13**, 63-79 (2014).
41. Light, D.W. & Kantarjian, H. Market spiral pricing of cancer drugs. *Cancer* **119**, 3900-3902 (2013).
42. Hay, M., Thomas, D.W., Craighead, J.L., Economides, C. & Rosenthal, J. Clinical development success rates for investigational drugs. *Nat Biotech* **32**, 40-51 (2014).
43. Quail, D.F. & Joyce, J.A. Microenvironmental regulation of tumor progression and metastasis. *Nature medicine* **19**, 1423-1437 (2013).
44. Bissell, M.J. & Hines, W.C. Why don't we get more cancer? A proposed role of the microenvironment in restraining cancer progression. *Nature medicine* **17**, 320-329 (2011).
45. Talmadge, J.E., Singh, R.K., Fidler, I.J. & Raz, A. Murine Models to Evaluate Novel and Conventional Therapeutic Strategies for Cancer. *The American journal of pathology* **170**, 793-804 (2007).
46. Egeblad, M., Nakasone, E.S. & Werb, Z. Tumors as organs: complex tissues that interface with the entire organism. *Developmental cell* **18**, 884-901 (2010).
47. Junttila, M.R. & de Sauvage, F.J. Influence of tumour micro-environment heterogeneity on therapeutic response. *Nature* **501**, 346-354 (2013).
48. Mlecnik, B. et al. The tumor microenvironment and Immunoscore are critical determinants of dissemination to distant metastasis. *Science translational medicine* **8**, 327ra326-327ra326 (2016).
49. Butcher, D.T., Alliston, T. & Weaver, V.M. A tense situation: forcing tumour progression. *Nat Rev Cancer* **9**, 108-122 (2009).

50. Correia, A.L. & Bissell, M.J. The tumor microenvironment is a dominant force in multidrug resistance. *Drug resistance updates : reviews and commentaries in antimicrobial and anticancer chemotherapy* **15**, 39-49 (2012).
51. Sneddon, J.B. & Werb, Z. Location, location, location: the cancer stem cell niche. *Cell stem cell* **1**, 607-611 (2007).
52. Yang, Z.J. & Wechsler-Reya, R.J. Hit 'em where they live: targeting the cancer stem cell niche. *Cancer Cell* **11**, 3-5 (2007).
53. Flynn, C.M. & Kaufman, D.S. Donor cell leukemia: insight into cancer stem cells and the stem cell niche. *Blood* **109**, 2688-2692 (2007).
54. Fuchs, E., Tumbar, T. & Guasch, G. Socializing with the Neighbors: Stem Cells and Their Niche. *Cell* **116**, 769-778 (2004).
55. Scadden, D.T. The stem-cell niche as an entity of action. *Nature* **441**, 1075-1079 (2006).
56. Collins, C.A. et al. Stem cell function, self-renewal, and behavioral heterogeneity of cells from the adult muscle satellite cell niche. *Cell* **122**, 289-301 (2005).
57. Nishimura, E.K. et al. Dominant role of the niche in melanocyte stem-cell fate determination. *Nature* **416**, 854-860 (2002).
58. Sacco, A., Doyonnas, R., Kraft, P., Vitorovic, S. & Blau, H.M. Self-renewal and expansion of single transplanted muscle stem cells. *Nature* **456**, 502-506 (2008).
59. Booth, B.W. et al. The mammary microenvironment alters the differentiation repertoire of neural stem cells. *Proc Natl Acad Sci U S A* **105**, 14891-14896 (2008).
60. Boulanger, C.A., Mack, D.L., Booth, B.W. & Smith, G.H. Interaction with the mammary microenvironment redirects spermatogenic cell fate in vivo. *Proceedings of the National Academy of Sciences of the United States of America* **104**, 3871-3876 (2007).
61. Flaim, C.J., Chien, S. & Bhatia, S.N. An extracellular matrix microarray for probing cellular differentiation. *Nat Meth* **2**, 119-125 (2005).
62. LaBarge, M.A. et al. Human mammary progenitor cell fate decisions are products of interactions with combinatorial microenvironments. *Integr Biol* **1**, 70-79 (2009).
63. Soen, Y., Mori, A., Palmer, T.D. & Brown, P.O. Exploring the regulation of human neural precursor cell differentiation using arrays of signaling microenvironments. *Molecular Systems Biology* **2**, 37-37 (2006).
64. Lin, C.H., Lee, J.K. & LaBarge, M.A. Fabrication and use of microenvironment microarrays (MEArrays). *J Vis Exp* (2012).
65. LaBarge, M.A., Petersen, O.W. & Bissell, M.J. Of microenvironments and mammary stem cells. *Stem cell reviews* **3**, 137-146 (2007).
66. LaBarge, M.A. The difficulty of targeting cancer stem cell niches. *Clinical cancer research : an official journal of the American Association for Cancer Research* **16**, 3121-3129 (2010).

67. Bissell, M.J. & LaBarge, M.A. Context, tissue plasticity, and cancer: Are tumor stem cells also regulated by the microenvironment? *Cancer cell* **7**, 17-23 (2005).
68. Kenny, P.A. & Bissell, M.J. Tumor reversion: Correction of malignant behavior by microenvironmental cues. *International Journal of Cancer* **107**, 688-695 (2003).
69. Levental, I., Georges, P.C. & Janmey, P.A. Soft biological materials and their impact on cell function. *Soft Matter* **3**, 299-306 (2007).
70. Hansen, K.C. et al. An in-solution ultrasonication-assisted digestion method for improved extracellular matrix proteome coverage. *Molecular & cellular proteomics : MCP* **8**, 1648-1657 (2009).
71. Zanella, F., Lorens, J.B. & Link, W. High content screening: seeing is believing. *Trends in biotechnology* **28**, 237-245 (2010).
72. Ranga, A. et al. 3D niche microarrays for systems-level analyses of cell fate. *Nature communications* **5** (2014).
73. Pelissier, F.A. et al. Age-related dysfunction in mechanotransduction impairs differentiation of human mammary epithelial progenitors. *Cell Rep* **7**, 1926-1939 (2014).
74. Shin, I., Park, S. & Lee, M.-r. Carbohydrate Microarrays: An Advanced Technology for Functional Studies of Glycans. *Chemistry – A European Journal* **11**, 2894-2901 (2005).
75. Brafman, D.A. et al. Investigating the role of the extracellular environment in modulating hepatic stellate cell biology with arrayed combinatorial microenvironments. *Integrative Biology* **1**, 513-524 (2009).
76. Lee, G.Y., Kenny, P.A., Lee, E.H. & Bissell, M.J. Three-dimensional culture models of normal and malignant breast epithelial cells. *Nature methods* **4**, 359-365 (2007).
77. Tse, J.R. & Engler, A.J. Preparation of hydrogel substrates with tunable mechanical properties. *Current protocols in cell biology / editorial board, Juan S. Bonifacino ... [et al.]* **Chapter 10**, Unit 10 16 (2010).
78. Jones, T.R. et al. CellProfiler Analyst: data exploration and analysis software for complex image-based screens. *BMC Bioinformatics* **9**, 1-16 (2008).
79. Team, R.C. R: A Language and Environment for Statistical Computing. (2015).
80. Hilsenbeck, S.G. et al. Statistical Analysis of Array Expression Data as Applied to the Problem of Tamoxifen Resistance. *Journal of the National Cancer Institute* **91**, 453-459 (1999).
81. Amir, E.-a.D. et al. viSNE enables visualization of high dimensional single-cell data and reveals phenotypic heterogeneity of leukemia. *Nat Biotech* **31**, 545-552 (2013).
82. Rosario-Martinez, H.D. phia: Post-Hoc Interaction Analysis. (2015).
83. Halder, G., Dupont, S. & Piccolo, S. Transduction of mechanical and cytoskeletal cues by YAP and TAZ. *Nature reviews. Molecular cell biology* **13**, 591-600 (2012).

84. Wang, X., Su, L. & Ou, Q. Yes-associated protein promotes tumour development in luminal epithelial derived breast cancer. *Eur J Cancer* **48**, 1227-1234 (2012).
85. Neve, R.M. et al. A collection of breast cancer cell lines for the study of functionally distinct cancer subtypes. *Cancer Cell* **10**, 515-527 (2006).
86. Burris, H.A., 3rd et al. Phase I safety, pharmacokinetics, and clinical activity study of lapatinib (GW572016), a reversible dual inhibitor of epidermal growth factor receptor tyrosine kinases, in heavily pretreated patients with metastatic carcinomas. *Journal of clinical oncology : official journal of the American Society of Clinical Oncology* **23**, 5305-5313 (2005).
87. Soofi, S.S., Last, J.A., Liliensiek, S.J., Nealey, P.F. & Murphy, C.J. The elastic modulus of Matrigel as determined by atomic force microscopy. *J Struct Biol* **167**, 216-219 (2009).
88. Saruwatari, L. et al. Osteoblasts generate harder, stiffer, and more delamination-resistant mineralized tissue on titanium than on polystyrene, associated with distinct tissue micro- and ultrastructure. *Journal of bone and mineral research : the official journal of the American Society for Bone and Mineral Research* **20**, 2002-2016 (2005).
89. Kolahi, K.S. et al. Effect of substrate stiffness on early mouse embryo development. *PloS one* **7**, e41717 (2012).
90. Holle, A.W. & Engler, A.J. More than a feeling: discovering, understanding, and influencing mechanosensing pathways. *Curr Opin Biotechnol* **22**, 648-654 (2011).
91. Liu-Chittenden, Y. et al. Genetic and pharmacological disruption of the TEAD-YAP complex suppresses the oncogenic activity of YAP. *Genes & development* **26**, 1300-1305 (2012).
92. Zhang, J. et al. YAP-dependent induction of amphiregulin identifies a non-cell-autonomous component of the Hippo pathway. *Nature cell biology* **11**, 1444-1450 (2009).
93. Higginbotham, J.N. et al. Amphiregulin exosomes increase cancer cell invasion. *Current biology : CB* **21**, 779-786 (2011).
94. Hurbin, A., Dubrez, L., Coll, J.L. & Favrot, M.C. Inhibition of apoptosis by amphiregulin via an insulin-like growth factor-1 receptor-dependent pathway in non-small cell lung cancer cell lines. *The Journal of biological chemistry* **277**, 49127-49133 (2002).
95. Yotsumoto, F. et al. Amphiregulin regulates the activation of ERK and Akt through epidermal growth factor receptor and HER3 signals involved in the progression of pancreatic cancer. *Cancer science* **101**, 2351-2360 (2010).
96. Garrett, J.T. et al. Transcriptional and posttranslational up-regulation of HER3 (ErbB3) compensates for inhibition of the HER2 tyrosine kinase. *Proc Natl Acad Sci U S A* **108**, 5021-5026 (2011).
97. Hobor, S. et al. TGF-alpha and amphiregulin paracrine network promotes resistance to EGFR blockade in colorectal cancer cells. *Clinical cancer research : an official journal of the American Association for Cancer Research* (2014).

98. LaBarge, M.A. et al. Human mammary progenitor cell fate decsions are products of interactions with combinatorial microenvironments. *Integrative Biology* **1**, 70-79 (2009).
99. Lamprecht, M.R., Sabatini, D.M. & Carpenter, A.E. CellProfiler: free, versatile software for automated biological image analysis. *Biotechniques* **42**, 71-75 (2007).
100. Pontiggia, O. et al. The tumor microenvironment modulates tamoxifen resistance in breast cancer: a role for soluble stromal factors and fibronectin through β1 integrin. *Breast cancer research and treatment* **133**, 459-471 (2012).
101. Yuan, J. et al. Acquisition of epithelial-mesenchymal transition phenotype in the tamoxifen-resistant breast cancer cell: a new role for G protein-coupled estrogen receptor in mediating tamoxifen resistance through cancer-associated fibroblast-derived fibronectin and β1-integrin signaling pathway in tumor cells. *Breast cancer research : BCR* **17**, 69 (2015).
102. Li, J. et al. TCPA: a resource for cancer functional proteomics data. *Nat Meth* **10**, 1046-1047 (2013).
103. Yuan, M. et al. Yes-associated protein (YAP) functions as a tumor suppressor in breast. *Cell Death Differ* **15**, 1752-1759 (2008).
104. Tufail, R., Jorda, M., Zhao, W., Reis, I. & Nawaz, Z. Loss of Yes-associated protein (YAP) expression is associated with estrogen and progesterone receptors negativity in invasive breast carcinomas. *Breast cancer research and treatment* **131**, 743-750 (2012).
105. Lamar, J.M. et al. The Hippo pathway target, YAP, promotes metastasis through its TEAD-interaction domain. *Proc Natl Acad Sci U S A* **109**, E2441-2450 (2012).
106. Kim, S.K., Jung, W.H. & Koo, J.S. Yes-associated protein (YAP) is differentially expressed in tumor and stroma according to the molecular subtype of breast cancer. *Int J Clin Exp Pathol* **7**, 3224-3234 (2014).
107. Calvo, F. et al. Mechanotransduction and YAP-dependent matrix remodelling is required for the generation and maintenance of cancer-associated fibroblasts. *Nature cell biology* **15**, 637-646 (2013).
108. Morin-Kensicki, E.M. et al. Defects in yolk sac vasculogenesis, chorioallantoic fusion, and embryonic axis elongation in mice with targeted disruption of Yap65. *Molecular and cellular biology* **26**, 77-87 (2006).
109. Hossain, Z. et al. Glomerulocystic kidney disease in mice with a targeted inactivation of Wwtr1. *Proc Natl Acad Sci U S A* **104**, 1631-1636 (2007).
110. Michels, S. & Schmidt-Erfurth, U. Photodynamic therapy with verteporfin: a new treatment in ophthalmology. *Seminars in ophthalmology* **16**, 201-206 (2001).
111. Zustiak, S., Nossal, R. & Sackett, D.L. Multiwell stiffness assay for the study of cell responsiveness to cytotoxic drugs. *Biotechnol Bioeng* **111**, 396-403 (2014).
112. Sharma, S., Santiskulvong, C., Rao, J., Gimzewski, J.K. & Dorigo, O. The role of Rho GTPase in cell stiffness and cisplatin resistance in ovarian cancer cells. *Integr Biol* **6**, 611-617 (2014).

113. Nguyen, T.V., Sleiman, M., Moriarty, T., Herrick, W.G. & Peyton, S.R. Sorafenib resistance and JNK signaling in carcinoma during extracellular matrix stiffening. *Biomaterials* **35**, 5749-5759 (2014).
114. Baker, B.M. & Chen, C.S. Deconstructing the third dimension - how 3D culture microenvironments alter cellular cues. *Journal of cell science* **125**, 3015-3024 (2012).
115. Labarge, M.A., Parvin, B. & Lorens, J.B. Molecular deconstruction, detection, and computational prediction of microenvironment-modulated cellular responses to cancer therapeutics. *Adv Drug Deliv Rev* **70**, 123-131 (2014).
116. Ankam, S., Teo, B.K., Kukumberg, M. & Yim, E.K. High throughput screening to investigate the interaction of stem cells with their extracellular microenvironment. *Organogenesis* **9**, 128-142 (2013).
117. Kuschel, C. et al. Cell adhesion profiling using extracellular matrix protein microarrays. *Biotechniques* **40**, 523-531 (2006).
118. Konagaya, S., Kato, K., Nakaji-Hirabayashi, T., Arima, Y. & Iwata, H. Array-based functional screening of growth factors toward optimizing neural stem cell microenvironments. *Biomaterials* **32**, 5015-5022 (2011).
119. Angenendt, P. Progress in protein and antibody microarray technology. *Drug discovery today* **10**, 503-511 (2005).
120. Kim, H. et al. Patterning Methods for Polymers in Cell and Tissue Engineering. *Ann Biomed Eng* **40**, 1339-1355 (2012).
121. Yang, Y.H. et al. Normalization for cDNA microarray data: a robust composite method addressing single and multiple slide systematic variation. *Nucleic Acids Research* **30**, e15 (2002).
122. Brafman, D.A., Chien, S. & Willert, K. Arrayed cellular microenvironments for identifying culture and differentiation conditions for stem, primary and rare cell populations. *Nat. Protocols* **7**, 703-717 (2012).
123. Guyon, L. et al. Φ-score: A cell-to-cell phenotypic scoring method for sensitive and selective hit discovery in cell-based assays. *Scientific reports* **5**, 14221 (2015).
124. Konagaya, S., Kato, K., Nakaji-Hirabayashi, T., Arima, Y. & Iwata, H. Array-based functional screening of growth factors toward optimizing neural stem cell microenvironments. *Biomaterials* **32**, 5015-5022 (2011).
125. Steinbach, M., Ertöz, L. & Kumar, V. in New Directions in Statistical Physics. (ed. L. Wille) 273-309 (Springer Berlin Heidelberg, 2004).
126. Bellman, R. Adaptive Control Processes: A Guided Tour. (Princeton University Press, Princeton, New Jersey; 1961).
127. Hilsenbeck, S.G. et al. Statistical analysis of array expression data as applied to the problem of tamoxifen resistance. *J Natl Cancer Inst* **91**, 453-459 (1999).
128. Scholz, M., Gatzek, S., Sterling, A., Fiehn, O. & Selbig, J. Metabolite fingerprinting: detecting biological features by independent component analysis. *Bioinformatics* **20**, 2447-2454 (2004).
129. Haykin, S. & Chen, Z. The cocktail party problem. *Neural computation* **17**, 1875-1902 (2005).

130. Yao, F., Coquery, J. & Le Cao, K.-A. Independent Principal Component Analysis for biologically meaningful dimension reduction of large biological data sets. *BMC Bioinformatics* **13**, 24 (2012).
131. Laurens van der Maaten, G.H. Visualizing data using t-SNE. *The Journal of Machine Learning Research* **9**, 2579-2605 (2008).
132. Bendall, S.C. et al. Single-Cell Mass Cytometry of Differential Immune and Drug Responses Across a Human Hematopoietic Continuum. *Science (New York, N.y.)* **332**, 687-696 (2011).
133. Qiu, P. et al. Extracting a cellular hierarchy from high-dimensional cytometry data with SPADE. *Nature biotechnology* **29**, 886-891 (2011).
134. Hughes, C.S., Postovit, L.M. & Lajoie, G.A. Matrigel: a complex protein mixture required for optimal growth of cell culture. *Proteomics* **10**, 1886-1890 (2010).
135. Novaro, V., Roskelley, C.D. & Bissell, M.J. Collagen-IV and laminin-1 regulate estrogen receptor α expression and function in mouse mammary epithelial cells. *Journal of cell science* **116**, 2975-2986 (2003).
136. Kim, N.-G. & Gumbiner, B.M. Adhesion to fibronectin regulates Hippo signaling via the FAK–Src–PI3K pathway. *The Journal of cell biology* **210**, 503-515 (2015).
137. Fernandez-Garcia, B. et al. Expression and prognostic significance of fibronectin and matrix metalloproteases in breast cancer metastasis. *Histopathology* **64**, 512-522 (2014).
138. Mak, I.W.Y., Evaniew, N. & Ghert, M. Lost in translation: animal models and clinical trials in cancer treatment. *American Journal of Translational Research* **6**, 114-118 (2014).
139. Bedard, P.L., Hansen, A.R., Ratain, M.J. & Siu, L.L. Tumour heterogeneity in the clinic. *Nature* **501**, 355-364 (2013).
140. Scholz, M., Gatzek, S., Sterling, A., Fiehn, O. & Selbig, J. Metabolite fingerprinting: detecting biological features by independent component analysis. *Bioinformatics* **20**, 2447 - 2454 (2004).

Chapter 7: Figures and figure legends

Figure 1. Substrata elastic modulus is a modifier of lapatinib responses in HER2-amplified cancer cells.

Bar graphs showing the relative incorporation of EdU expressed as a percentage of DMSO-treated cells in: (A) HCC1569 and BT549 cultured on 2D tissue culture plastic (TCP) dishes or 3D in Matrigel for 48 h, and then treated with lapatinib or DMSO for 48 h (n = 3, 500 cells/condition/experiment, * $p < 0.05$). (B) Representative images of HCC1569 and BT549 cultured on 2D TCP or in 3D Matrigel. EdU is pseudocolored red, and nuclear DNA is blue. (C) Bar graphs showing relative incorporation of EdU expressed as a percentage of DMSO-treated cells. HCC1569 and BT549 cultured on 2D TCP or 400 Pa polyacrylamide (PA) gels for 48 h, followed by lapatinib (1.5 μM) or DMSO for 48 h (n = 3, 500 cells/condition/experiment, * $p < 0.05$). (D) Representative images of HCC1569 and BT549 cultured on 2D TCP or 400 Pa PA gels. EdU is pseudocolored red, and nuclear DNA is blue. Scale bars represent 20 μm. (E) Dose-response curves used to calculate IC50 of lapatinib in HCC1569 cultured on 400 Pa PA gel (0.94 μM) versus 2D TCP (2.66 μM). (n = 3, 500 cells/condition/experiment, * $p < 0.05$)[39].

Figure 1

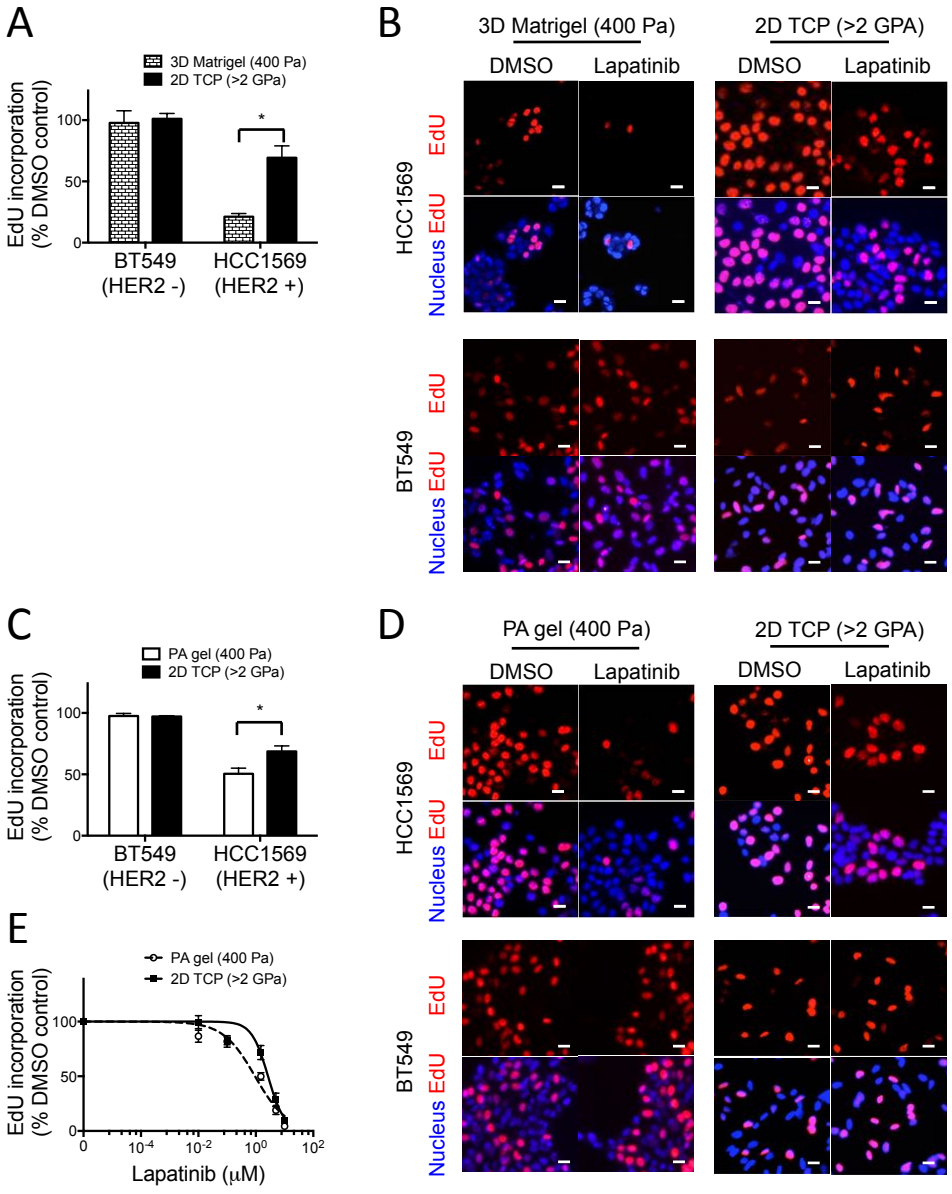
A
3D Matrigel (400 Pa)
2D TCP (>2 GPa)
EdU incorporation (% DMSO control)
100
50
0
*
BT549 (HER2 -)
HCC1569 (HER2 +)
B
3D Matrigel (400 Pa)
2D TCP (>2 GPA)
DMSO
Lapatinib
DMSO
Lapatinib
HCC1569
EdU
Nucleus EdU
BT549
EdU
Nucleus EdU
C
PA gel (400 Pa)
2D TCP (>2 GPa)
EdU incorporation (% DMSO control)
100
50
0
*
BT549 (HER2 -)
HCC1569 (HER2 +)
D
PA gel (400 Pa)
2D TCP (>2 GPA)
DMSO
Lapatinib
DMSO
Lapatinib
HCC1569
EdU
Nucleus EdU
BT549
EdU
Nucleus EdU
E
PA gel (400 Pa)
2D TCP (>2 GPa)
EdU incorporation (% DMSO control)
100
50
0
0
10-4
10-2
100
102
Lapatinib (μM)

Figure 2. Inhibition of ROCK1/2 and myosin II increases resistance to lapatinib on compliant substrata but has no effect in 3D matrigel.

Bar graphs showing the relative incorporation of EdU expressed as a percentage of DMSO-treated cells in response to 1.5mM lapatinib on 400 Pa or >2 GPa substrata in the presence of (A) Y27632 (10mM) or (B) blebbistatin (10mM). Bar graphs showing relative incorporation of EdU expressed as a percentage of DMSO-treated cells in response to 1.5mM lapatinib on 400 Pa or Matrigel substrata in the presence of (C) Y27632 (10mM) or (D) blebbistatin (10mM) * indicates $p < 0.05$.

Figure 2

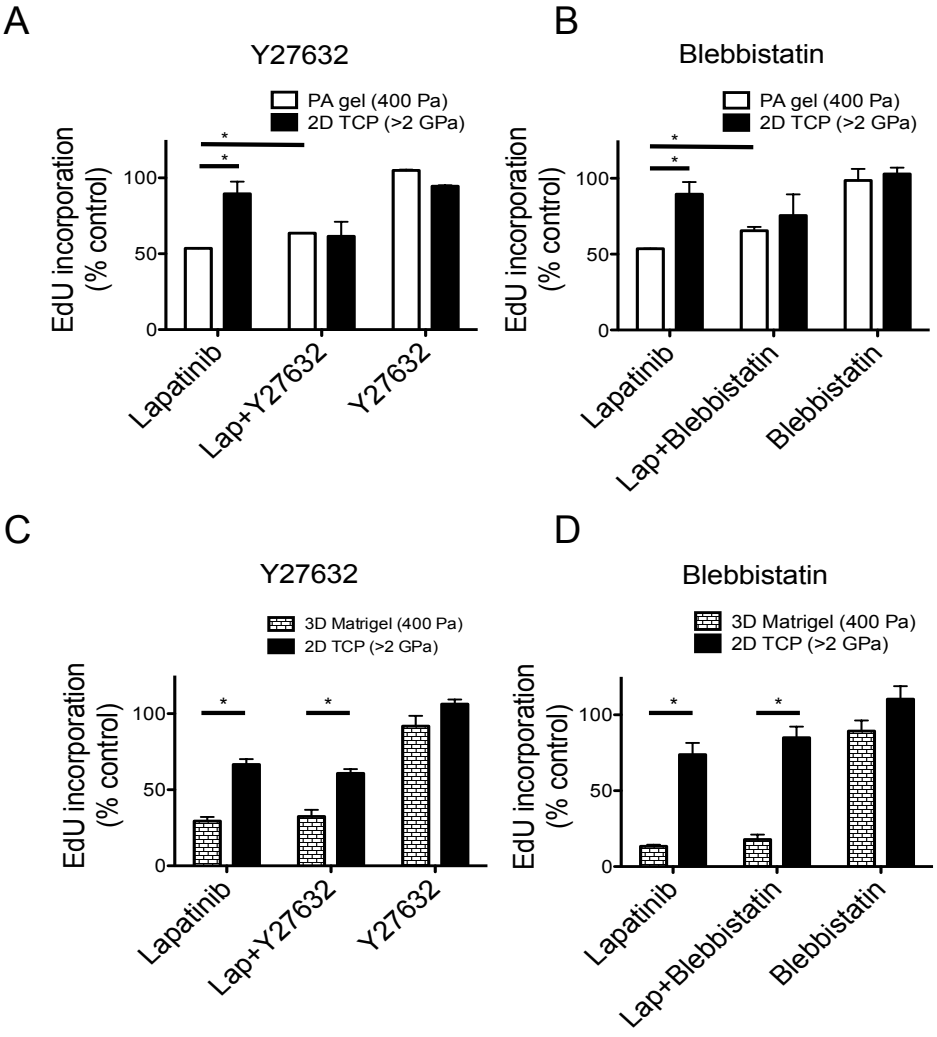
A
Y27632
PA gel (400 Pa)
2D TCP (>2 GPa)
EdU incorporation (% control)
100
50
0
*
*
Lapatinib
Lap+Y27632
Y27632
B
Blebbistatin
PA gel (400 Pa)
2D TCP (>2 GPa)
EdU incorporation (% control)
100
50
0
*
*
Lapatinib
Lap+Blebbistatin
Blebbistatin
C
Y27632
3D Matrigel (400 Pa)
2D TCP (>2 GPa)
EdU incorporation (% control)
100
50
0
*
*
Lapatinib
Lap+Y27632
Y27632
D
Blebbistatin
3D Matrigel (400 Pa)
2D TCP (>2 GPa)
EdU incorporation (% control)
100
50
0
*
*
Lapatinib
Lap+Blebbistatin
Blebbistatin

Figure 3. YAP and TAZ are required for the modulus-dependent lapatinib responses.

(A) Representative images of HCC1569 after 48 h cultured on substrata of increasing stiffness: immunofluorescence stains represent YAP (green), TAZ (red), and nucleus (blue). Scale bars represent 20 μm. (B) Bar graphs showing the proportions of single cells in which YAP and TAZ were located in the nucleus, cytoplasm, or evenly distributed in both compartments, as a function of stiffness (n = 3, 100 cells/condition/ experiment, * $p < 0.05$). (C) Bar graphs showing the relative incorporation of EdU in HCC1569 cultured on 2D TCP and 400 Pa PA gel with YAP or TAZ knockdown by siRNA for 72 h, and then treated with lapatinib (1.5 μM) or DMSO for 48 h. Results are expressed as a percentage of cells treated with DMSO and non-silencing control (NSC) siRNA-treated cells (n = 3, 500 cells/condition/experiment, * $p < 0.05$), (D) Bar graphs showing relative incorporation of EdU in HCC1569 cultured on 400 Pa and 40 kPa PA gels for 48 h, and then treated with lapatinib (1.5 μM) together with verteporfin (2 μg/mL), or DMSO for 48 h. Results expressed as percentage of DMSO treated controls (n = 3, 500/condition/experiment, * $p < 0.05$)[39].

Figure 3

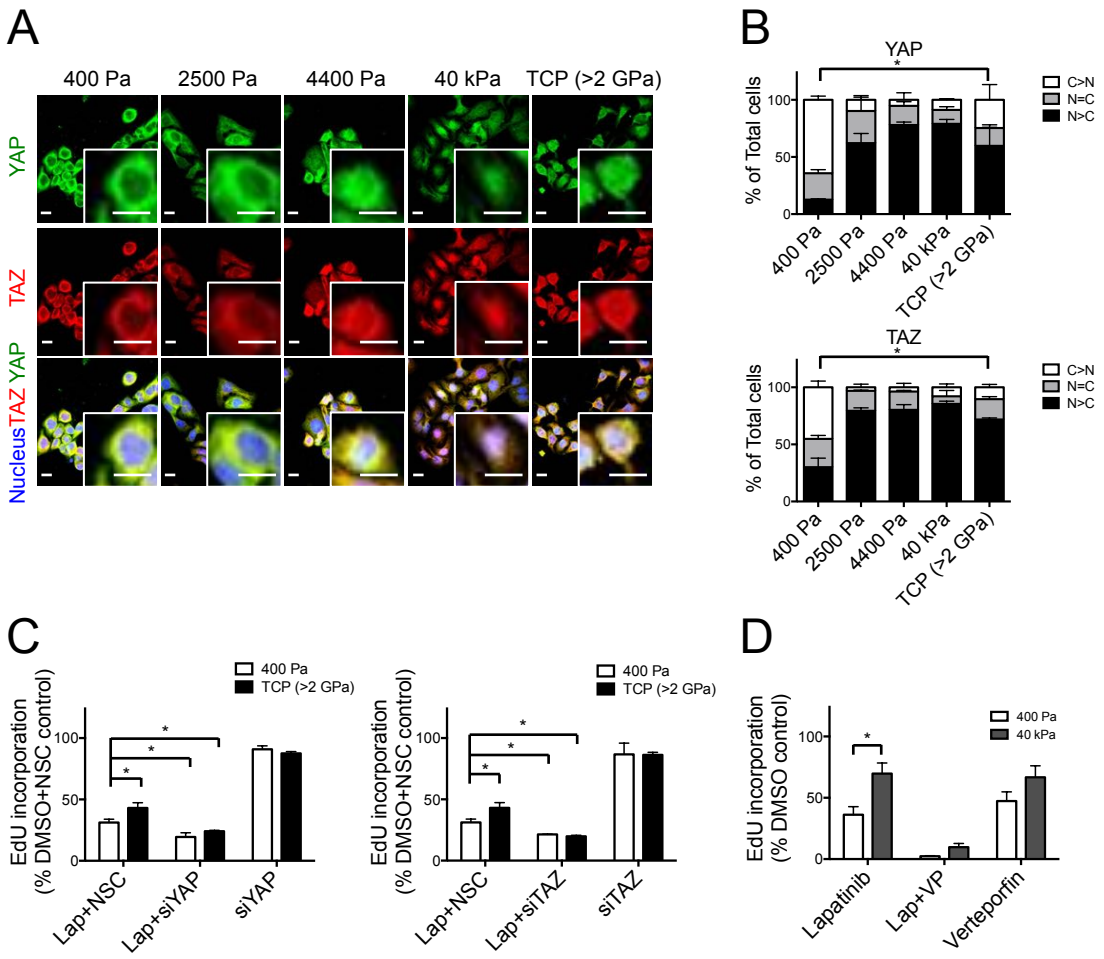
A
400 Pa
2500 Pa
4400 Pa
40 kPa
TCP (>2 GPa)
YAP
TAZ
Nucleus TAZ YAP
B
YAP
% of Total cells
C>N
N=C
N>C
400 Pa
2500 Pa
4400 Pa
40 kPa
TCP (>2 GPa)
TAZ
C
EdU incorporation (% DMSO+NSC control)
400 Pa
TCP (>2 GPa)
Lap+NSC
Lap+siYAP
siYAP
Lap+siTAZ
siTAZ
D
400 Pa
40 kPa
Lapatinib
Lap+VP
Verteporfin

Figure 4. YAP knockdown has synergistic trend of inhibition with lapatinib *in vivo*.

Tumor volume curves as a function of time and the summary table of area under curve (AUC) data for different treatment groups. The tumor volume was measured during the course of lapatinib treatment on mice that did not receive IPTG or lapatinib (group A), mice treated with IPTG only (group B), mice treated with lapatinib only (group C), and mice treated with lapatinib together with IPTG (group D)[39].

Figure 4

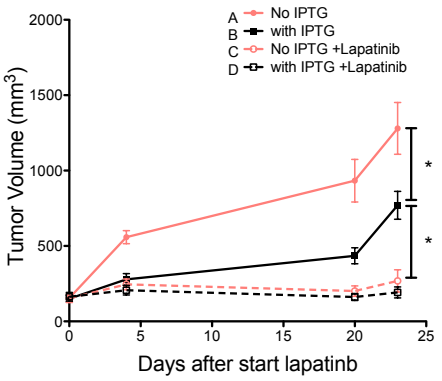

Summary of AUC data

	No IPTG	with IPTG	No IPTG +Lapatinib	with IPTG +Lapatinib
Number of values	9	10	10	10
Minimum	11947	4480	1149	1751
25% Percentile	12757	6177	2626	2843
Median	15820	7720	5811	3801
75% Percentile	21299	10862	7158	5350
Maximum	24153	14308	7368	7334
Mean	16680	8372	4938	4171
Std. Deviation	4747	3069	2359	1859
Std. Error	1582	970.5	745.9	587.8
Lower 95% CI	13031	6177	3250	2841
Upper 95% CI	20328	10567	6625	5501

Figure 5. YAP-dependent amphiregulin protein regulation is involved in the modulus-dependent lapatinib responses.

Bar graphs showing (A) AREG mRNA expression level measured by qRT-PCR and (B) cell surface AREG measured by FACS in HCC1569 on TCP or 400 Pa PA gels for 96 h (n = 3, 10000 cells/condition/experiment, * $p < 0.05$). (C) Bar graphs showing the proportions of single cells in which YAP and TAZ were located in the nucleus, cytoplasm, or evenly distributed in both compartments, as a function of stiffness in HCC1569 cultured on TCP or 400 Pa PA gel for 48 h, and then treated with AREG (5 ng/mL) for 48 h (n = 3, 100 cells/condition/experiment, * $p < 0.05$). (D) Bar graphs showing the relative incorporation of EdU, expressed as a percentage of DMSO-treated cells in HCC1569 cultured on TCP or 400 Pa PA gels for 48 h, and then treated with lapatinib (1.5 mM), AREG (5 ng/mL), and erlotinib (1.5 mM) for 48 h (n = 3, 500 cells/condition/experiment, * $p < 0.05$). (E) Bar graphs showing intracellular AREG protein levels measured by ELISA in HCC1569 with NSC siRNA or YAP knockdown by siRNA for 72 h (n = 3, * $p < 0.05$). (F) Bar graphs show the relative incorporation of EdU, expressed as a percentage of (DMSO and NSC siRNA)-treated cells in HCC1569 cultured on 400 Pa and 40 kPa PA gel with AREG knockdown by siRNA for 72 h, and then treated with lapatinib (1.5 μM) or DMSO for 48 h (n = 3, 500 cells/condition/experiment, * $p < 0.05$)[39].

Figure 5

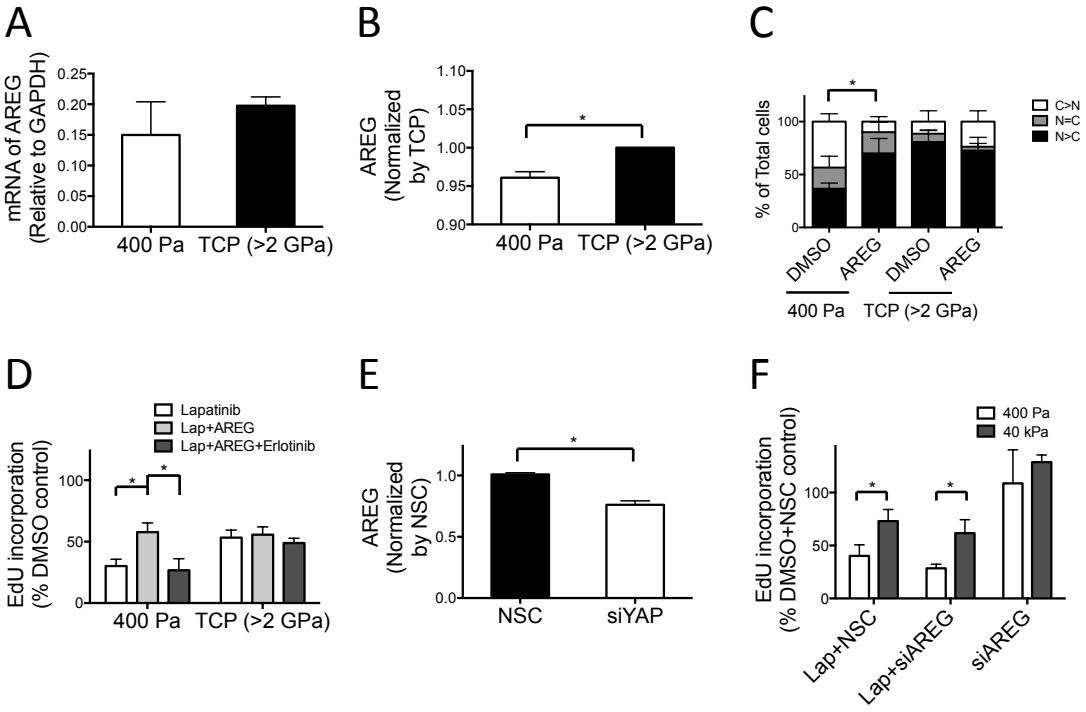
A
mRNA of AREG (Relative to GAPDH)
0.25
0.20
0.15
0.10
0.05
0.00
400 Pa
TCP (>2 GPa)
B
AREG (Normalized by TCP)
1.10
1.05
1.00
0.95
0.90
*
400 Pa
TCP (>2 GPa)
C
% of Total cells
100
50
0
*
C>N
N=C
N>C
DMSO
AREG
DMSO
AREG
400 Pa
TCP (>2 GPa)
D
Lapatinib
Lap+AREG
Lap+AREG+Erlotinib
EdU incorporation (% DMSO control)
100
50
0
*
*
400 Pa
TCP (>2 GPa)
E
AREG (Normalized by NSC)
1.0
0.5
0.0
*
NSC
siYAP
F
400 Pa
40 kPa
EdU incorporation (% DMSO+NSC control)
100
50
0
*
*
Lap+NSC
Lap+siAREG
siAREG

Figure 6. Knockdown efficiency in siRNA experiments.

(A) Expression levels of YAP and TAZ measured by qRT-PCR in HCC1569 with NSC siRNA, YAP or TAZ knockdown by siRNA for 72 h. (B) Fold change of expression levels of various receptors and ligands of the HER family were measured by qRT-PCR in HCC1569 with NSC siRNA or AREG knockdown by siRNA after 72 h[39].

Figure 6

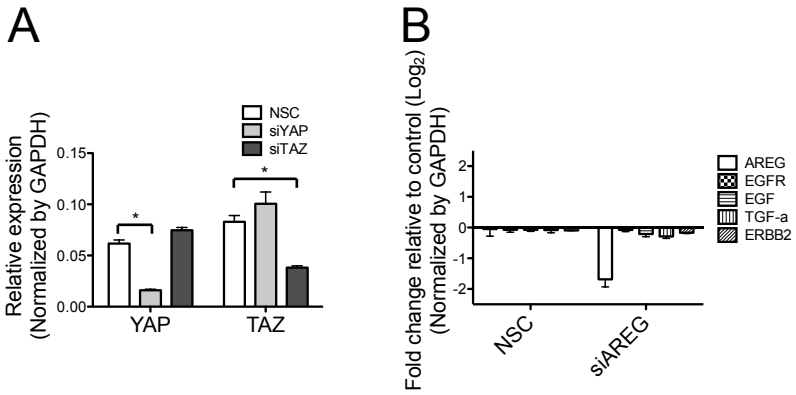
A
B
NSC
siYAP
siTAZ
Relative expression
(Normalized by GAPDH)
0.15
0.10
0.05
0.00
*
*
YAP
TAZ
Fold change relative to control (Log2)
(Normalized by GAPDH)
2
1
0
-1
-2
AREG
EGFR
EGF
TGF-a
ERBB2
NSC
siAREG

Figure 7. Verteporfin has a synergistic effect with lapatinib.

Line graphs show the relative incorporation of EdU, expressed as a percentage of DMSO-treated cells in HCC1569 cultured on 400 Pa or 40 kPa PA gels for 48 h, and then treated with lapatinib (1.5 μM) together with verteporfin (0, 0.2, 2, 10 μg/mL), or DMSO for 48 h. (n = 3, 500 cells/condition/experiment, * $p < 0.05$)[39].

Figure 7

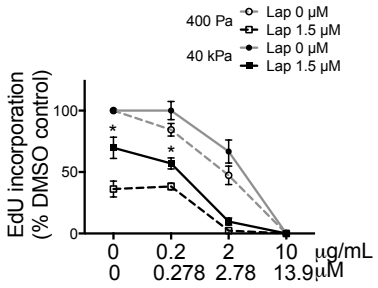
400 Pa
Lap 0 µM
Lap 1.5 µM
40 kPa
Lap 0 µM
Lap 1.5 µM
EdU incorporation
(% DMSO control)
100
50
0
*
*
0 0.2 2 10 µg/mL
0 0.278 2.78 13.9µM

Figure 8. Correlation between YAP gene expression with expression of a number of Hippo and HER-related genes in the TCGA dataset.

Summary table showing correlation between *YAP* and *ERBB2* gene expression with the other indicated genes. Pearson's r statistic is shown. Below, regression plots showing examples of the fit for all tumor types[39].

Figure 8

		AREG	TAZ	ERBB2	EGFR	ERBB3	CTGF
YAP	Pearson r	0.0825	0.3307	-0.05704	0.3713	-0.2447	0.3115
	P value	0.0452	< 0.0001	0.1664	< 0.0001	< 0.0001	< 0.0001
	Significant	*	***	ns	***	***	***
		AREG	**TAZ**	**YAP**	**EGFR**	**ERBB3**	**CTGF**
ERBB2	Pearson r	0.08503	-0.1244	-0.05704	-0.2654	0.3689	-0.02014
	P value	0.039	0.0025	0.1664	< 0.0001	< 0.0001	0.6253
	Significant	*	**	ns	***	***	ns

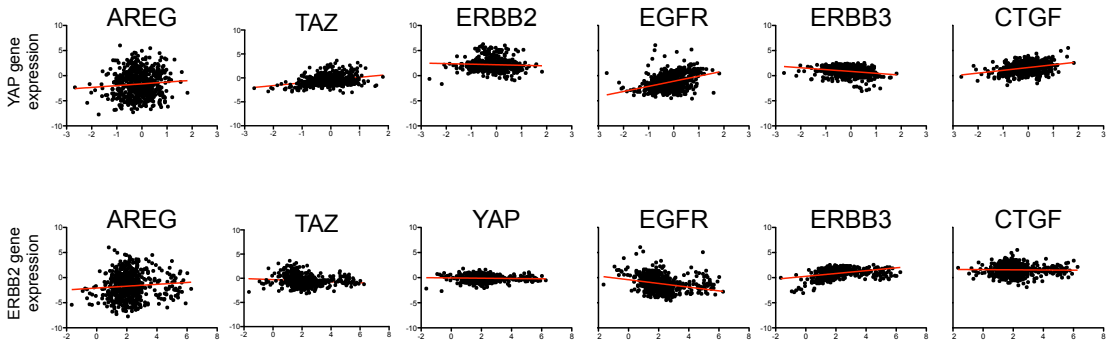

Figure 9. Responses to changes in microenvironmental stiffness for 49 different receptor tyrosine kinases (RTK).

(A) Images of RTK array membranes that were probed with extracts from HCC1569 cells. HCC1569 were grown for 48 h on 400 Pa or 40 kPa PA gel for 48 h, treated with lapatinib (1.5 μM) or DMSO, and then harvested at 1 h or 48 h after lapatinib treatment. (B) Bar graphs showing quantification of intensity of phosphorylation on EGFR, HER2, HER3, VEGFR1, and RYK RTKs. (C) A complete table of the RTKs represented on the blot[39].

Figure 9

A

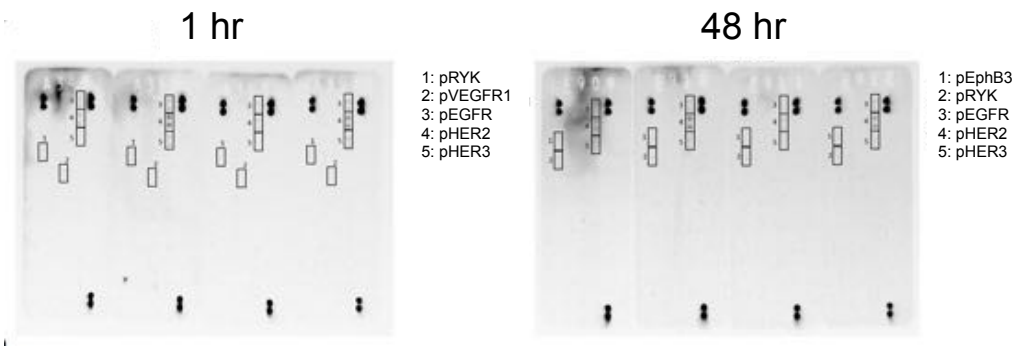

B

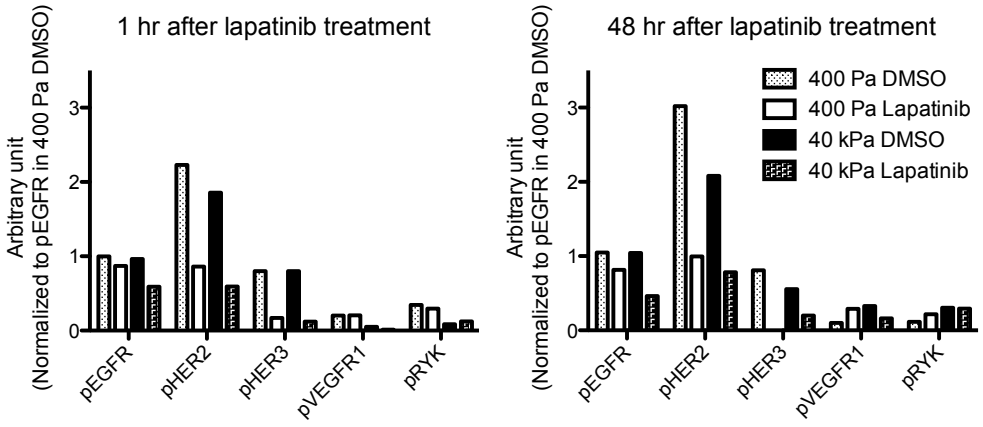

C

Human Phospho-RTK Array Coordinates

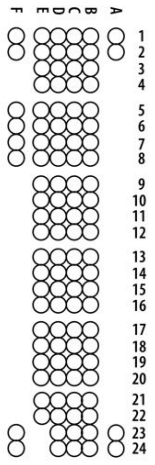

Refer to the table below for the Human Phospho-RTK Array coordinates.

Coordinate	Receptor Family	RTK/Control	Coodinate	Receptor Family	RTK/Control
A1, A2	Reference Spots	——	D1, D2	Tie	Tie-2
A23, A24	Reference Spots	——	D3, D4	NGF R	TrkA
B1, B2	EGF R	EGF R	D5, D6	NGF R	TrkB
B3, B4	EGF R	ErbB2	D7, D8	NGF R	TrkC
B5, B6	EGF R	ErbB3	D9, D10	VEGF R	VEGF R1
B7, B8	EGF R	ErbB4	D11, D12	VEGF R	VEGF R2
B9, B10	FGF R	FGF R1	D13, D14	VEGF R	VEGF R3
B11, B12	FGF R	FGF R2α	D15, D16	MuSK	MuSK
B13, B14	FGF R	FGF R3	D17, D18	Eph R	EphA1
B15, B16	FGF R	FGF R4	D19, D20	Eph R	EphA2
B17, B18	Insulin R	Insulin R	D21, D22	Eph R	EphA3
B19, B20	Insulin R	IGF-I R	D23, D24	Eph R	EphA4
B21, B22	Axl	Axl	E1, E2	Eph R	EphA6
B23, B24	Axl	Dtk	E3, E4	Eph R	EphA7
C1, C2	Axl	Mer	E5, E6	Eph R	EphB1
C3, C4	HGF R	HGF R	E7, E8	Eph R	EphB2
C5, C6	HGF R	MSP R	E9, E10	Eph R	EphB4
C7, C8	PDGF R	PDGF Rα	E11, E12	Eph R	EphB6
C9, C10	PDGF R	PDGF Rβ	E13, E14	Insulin R	ALK
C11, C12	PDGF R	SCF R	E15, E16	——	DDR1
C13, C14	PDGF R	Flt-3	E17, E18	——	DDR2
C15, C16	PDGF R	M-CSF R	E19, E20	Eph R	EphA5
C17, C18	RET	c-Ret	E21, E22	Eph R	EphA10
C19, C20	ROR	ROR1	F1, F2	Reference Spots	——
C21, C22	ROR	ROR2	F5, F6	Eph R	EphB3
C23, C24	Tie	Tie-1	F7, F8	——	RYK
			F23, F24	Control (-)	PBS

Figure 10. A flow chart of the MEArray procedure.

First, the printing substrata are prepared either with PDMS or PA. Second, the master plates are prepared and annotated in a database. Third, the MEArrays are printed and encoded with serial numbers. Fourth, culture chambers are attached, surfaces are blocks and/or rinsed, then cells are allowed to attach and unbound cells are washed away[64].

Figure 10

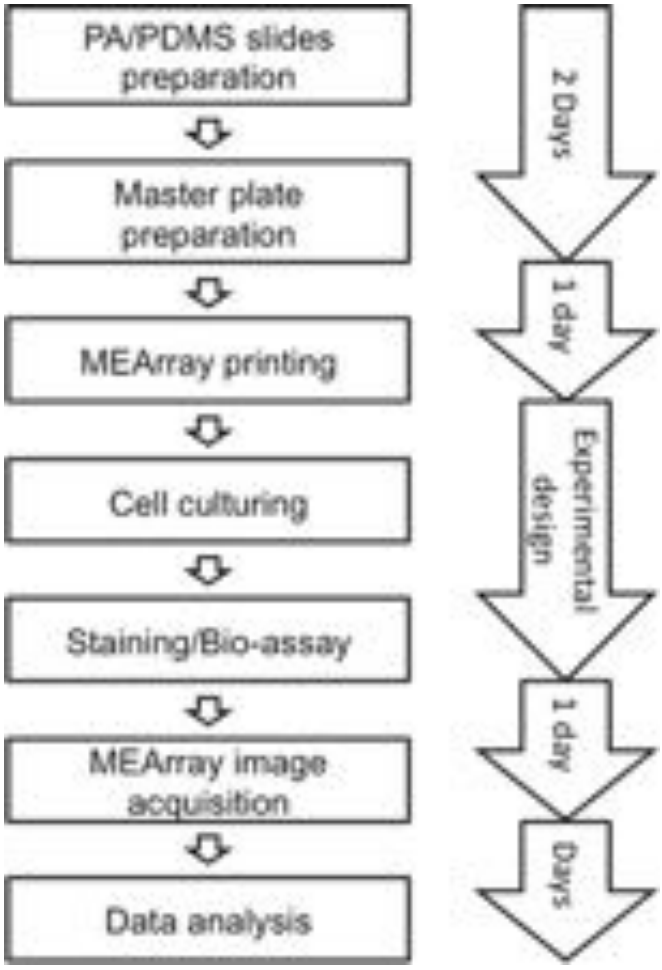
PA/PDMS slides preparation
Master plate preparation
MEArray printing
Cell culturing
Staining/Bio-assay
MEArray image acquisition
Data analysis
2 Days
1 day
Experimental design
1 day
Days

Figure 11. Deposition and relative abundance of printed proteins can be verified with immunostaining prior to cell attachment.

Antibodies that recognized type IV collagen and laminin-111 were used to verify their presence in printed features of an MEArray[64].

Figure 11

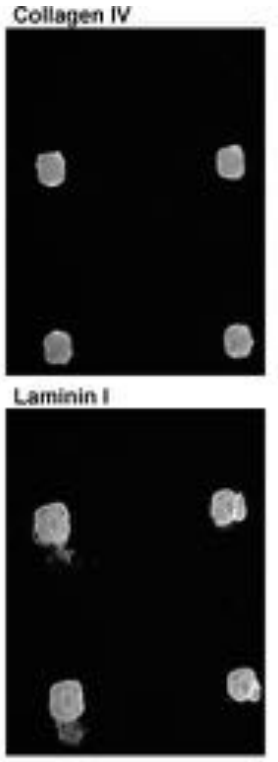

Figure 12. Deposition and relative abundance of printed proteins can be verified with immunostaining prior to cell attachment.

Using an average pixel intensity analysis feature in NIH ImageJ software, the relative abundance of the two proteins across a series of dilutions, starting from a 200 mg/mL protein solution, can be qualitatively assessed[64].

Figure 12

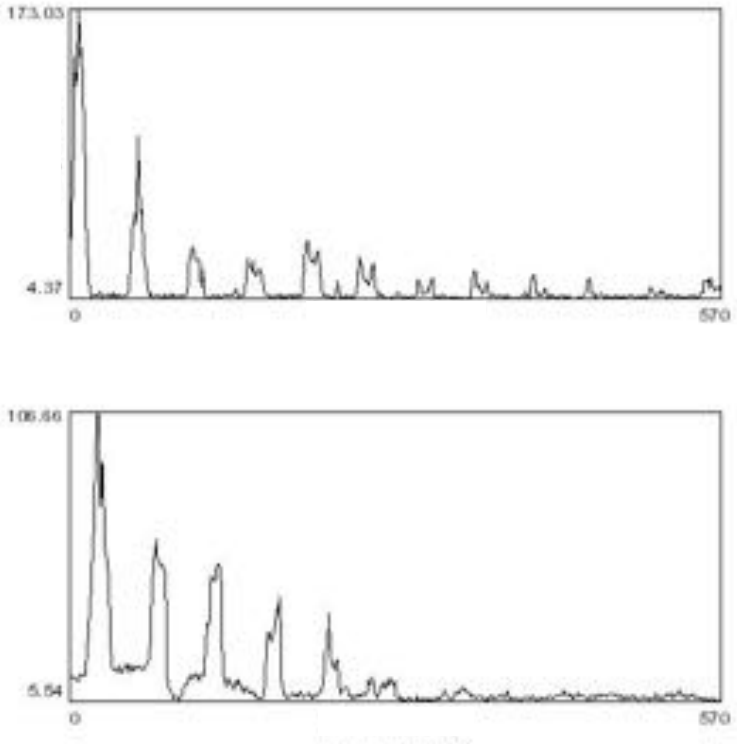

Figure 13. Deposition and relative abundance of printed proteins can be verified with immunostaining prior to cell attachment.

Phase micrograph of D920 cells attached to square-shaped features of a printed PDMS-coated MEArray[64].

Figure 13

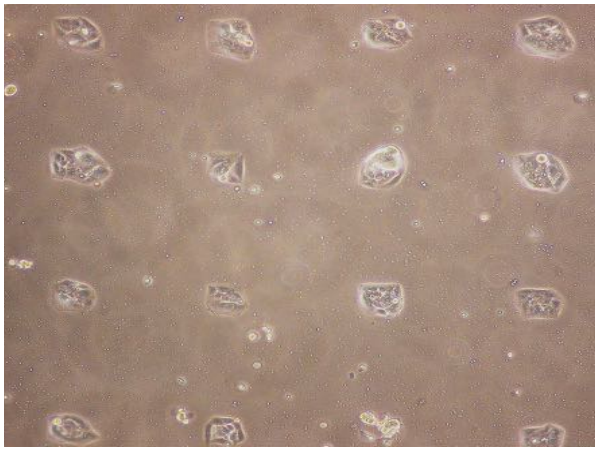

Figure 14. An example of an MEArray analysis using changes in keratin expression in a multipotent progenitor cell line as a functions of time and microenvironment.

Each bubble represents ratios of keratin 8 and keratin 14 protein levels from 10-15 cells attached to a feature in a MEArray. It shows the keratin ratios after 24 hours on an array that was plated in parallel. The maximum concentration of both proteins was 200mg/mL and diluted 2-fold. The diameter of a bubble represents the magnitude of the $\log_2$ ratio of keratin 8 and keratin 14 mean intensity, and the orange and white color-coding indicates values >0 and <0, respectively. F-values for one-way ANOVA and P-values from T-tests, and brackets with arrows identifying the populations compared, are shown[64].

Figure 14

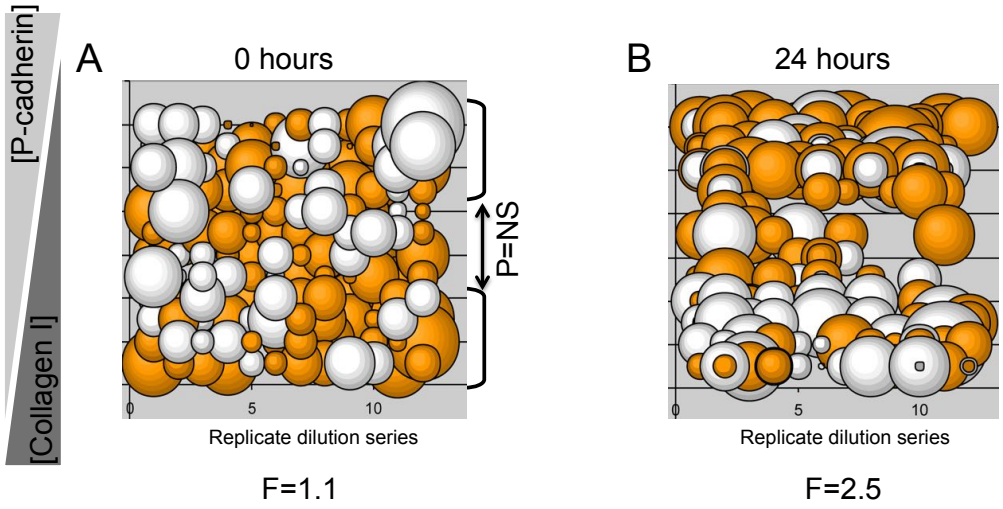
[P-cadherin]
[Collagen I]
A
0 hours
P=NS
0
5
10
Replicate dilution series
F=1.1
B
24 hours
0
5
10
Replicate dilution series
F=2.5

Figure 15. An example of an MEArray scan acquired using a tiled acquisition mode on a laser scanning confocal microscope.

HCC1569 cells we allowed to incorporate the DNA analog EdU for 4 hour prior to fixation. DAPI (blue) and EdU (red) are shown[64].

Figure 15

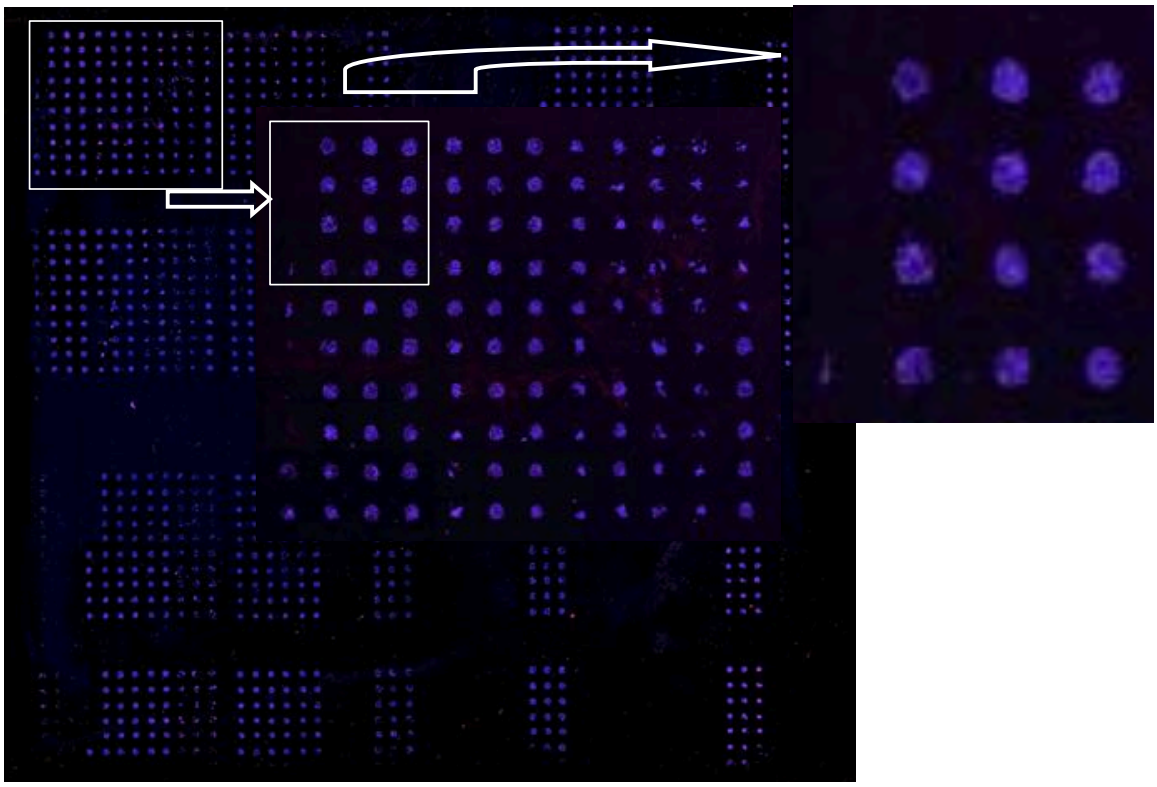

HCC1569 on 40,000Pa PA gel
MEArray
Blue = DAPI, Red = EdU

Figure 16. Both molecular compositions and matrix rigidity alter morphological features.

(A) A summary for a MEArray experiment. The total defined conditions were constructed by 4 Major ECM, 7 recombinant proteins, 2 matrix rigidity, and 2 drug treatments plus DMSO as control. The outcomes are cellular morphological measurements, immunofluorescence staining of targeted proteins, and functional analysis. (B) A representative image of MEArray. ViSNE was used for visualization of MEArray data. Each dot represents one defined microenvironment and color represents either (C) matrix rigidity or (D) major ECM composition. PCA analysis was used for identifying major variants. Each dot represents one defined microenvironment, and color represents either (E) matrix rigidity or (F) major ECM composition.

Figure 16

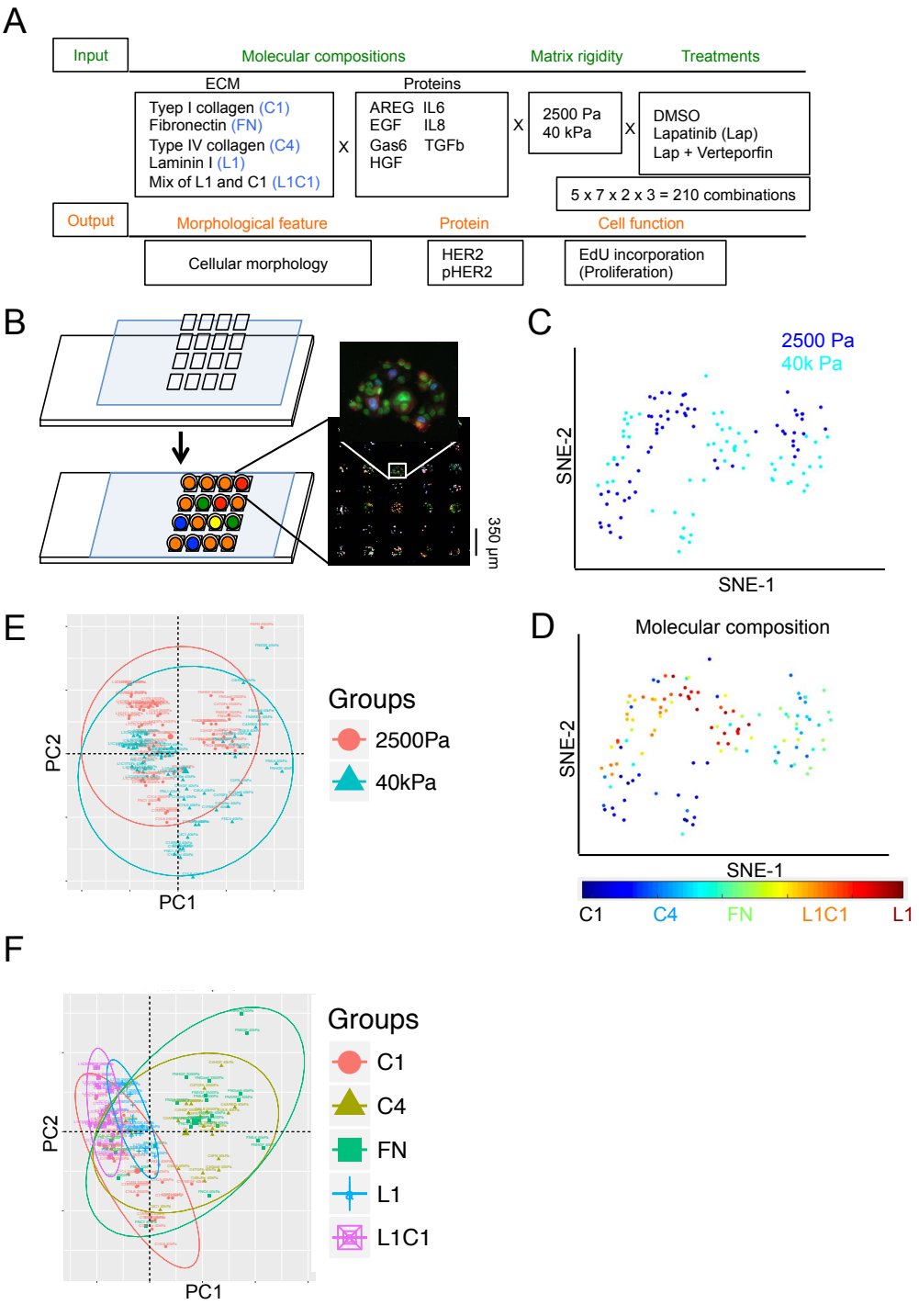
A
Input
Molecular compositions
Matrix rigidity
Treatments
ECM
Proteins
Tyep I collagen (C1)
Fibronectin (FN)
Type IV collagen (C4)
Laminin I (L1)
Mix of L1 and C1 (L1C1)
X
AREG IL6
EGF IL8
Gas6 TGFb
HGF
X
2500 Pa
40 kPa
X
DMSO
Lapatinib (Lap)
Lap + Verteporfin
5 x 7 x 2 x 3 = 210 combinations
Output
Morphological feature
Protein
Cell function
Cellular morphology
HER2
pHER2
EdU incorporation
(Proliferation)
B
350 µm
C
2500 Pa
40k Pa
SNE-2
SNE-1
D
Molecular composition
SNE-2
SNE-1
C1
C4
FN
L1C1
L1
E
PC2
PC1
Groups
2500Pa
40kPa
F
PC2
PC1
Groups
C1
C4
FN
L1
L1C1

Figure 17. The number of neighbor cells and cellular morphology were highly impacted by microenvironments.

A PCA analysis showing the major variants, such as number of neighbor cells, and cell morphology parameters, that were affected by microenvironments in the first and second PCA axis. A bar graph showing the major variants in the first dimension of PCA analysis.

Figure 17

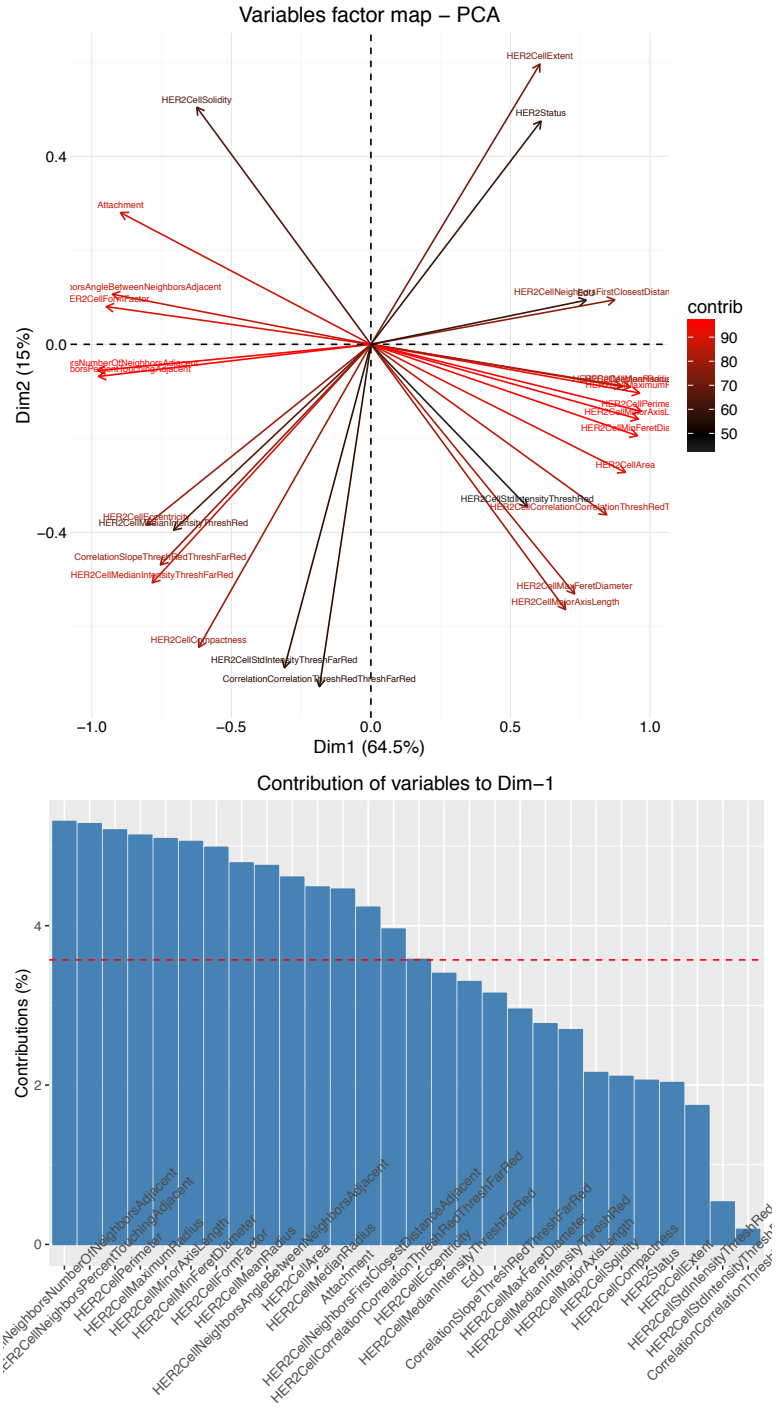
Variables factor map – PCA
HER2CellExtent
HER2CellSolidity
HER2Status
Attachment
HER2CellArea
HER2CellStdIntensityThreshRed
HER2CellMaxFeretDiameter
HER2CellMinorAxisLength
HER2CellCompactness
HER2CellStdIntensityThreshFarRed
CorrelationCorrelationThreshRedThreshFarRed
CorrelationSlopeThreshRedThreshFarRed
HER2CellMedianIntensityThreshFarRed
contrib
90
80
70
60
50
0.4
0.0
−0.4
−1.0
−0.5
0.0
0.5
1.0
Dim2 (15%)
Dim1 (64.5%)
Contribution of variables to Dim−1
Contributions (%)
4
2
0
HER2CellNeighborsNumberOfNeighborsAdjacent
HER2CellNeighborsPercentTouchingAdjacent
HER2CellPerimeter
HER2CellMaximumRadius
HER2CellMinorAxisLength
HER2CellFormFactor
HER2CellMeanRadius
HER2CellNeighborsAngleBetweenNeighborsAdjacent
HER2CellArea
HER2CellMedianRadius
Attachment
HER2CellNeighborsFirstClosestDistanceAdjacent
HER2CellCorrelationCorrelationThreshRedThreshFarRed
HER2CellEccentricity
HER2CellMedianIntensityThreshFarRed
EdU
CorrelationSlopeThreshRedThreshFarRed
HER2CellMaxFeretDiameter
HER2CellMedianIntensityThreshRed
HER2CellMajorAxisLength
HER2CellSolidity
HER2Status
HER2CellExtent
HER2CellStdIntensityThreshRed
HER2CellStdIntensityThreshFarRed
CorrelationCorrelationThreshRedThreshRed

Figure 18. The combined treatment of lapatinib and verteporfin had more inhibition on cells cultured on 2500 Pa substrate. Each point in ViSNE plot represents one defined microenvironment. Different color represents different matrix rigidity and drug treatment (A), different molecular combination (B), or different sensitivity to drug treatment (C). (D) The same data was normalized by z-score (A z-score of 0 is the mean, and the positive and the negative z-score indicating above or below the mean and by how many standard deviation), and plotted as heat map. In heat map, different color represents different major ECM in top-legend and represents lapatinib sensitivity in lower-legend (blue is sensitive, and red is resistant). (E) The heat map was plotted as sub-groups.

Figure 18

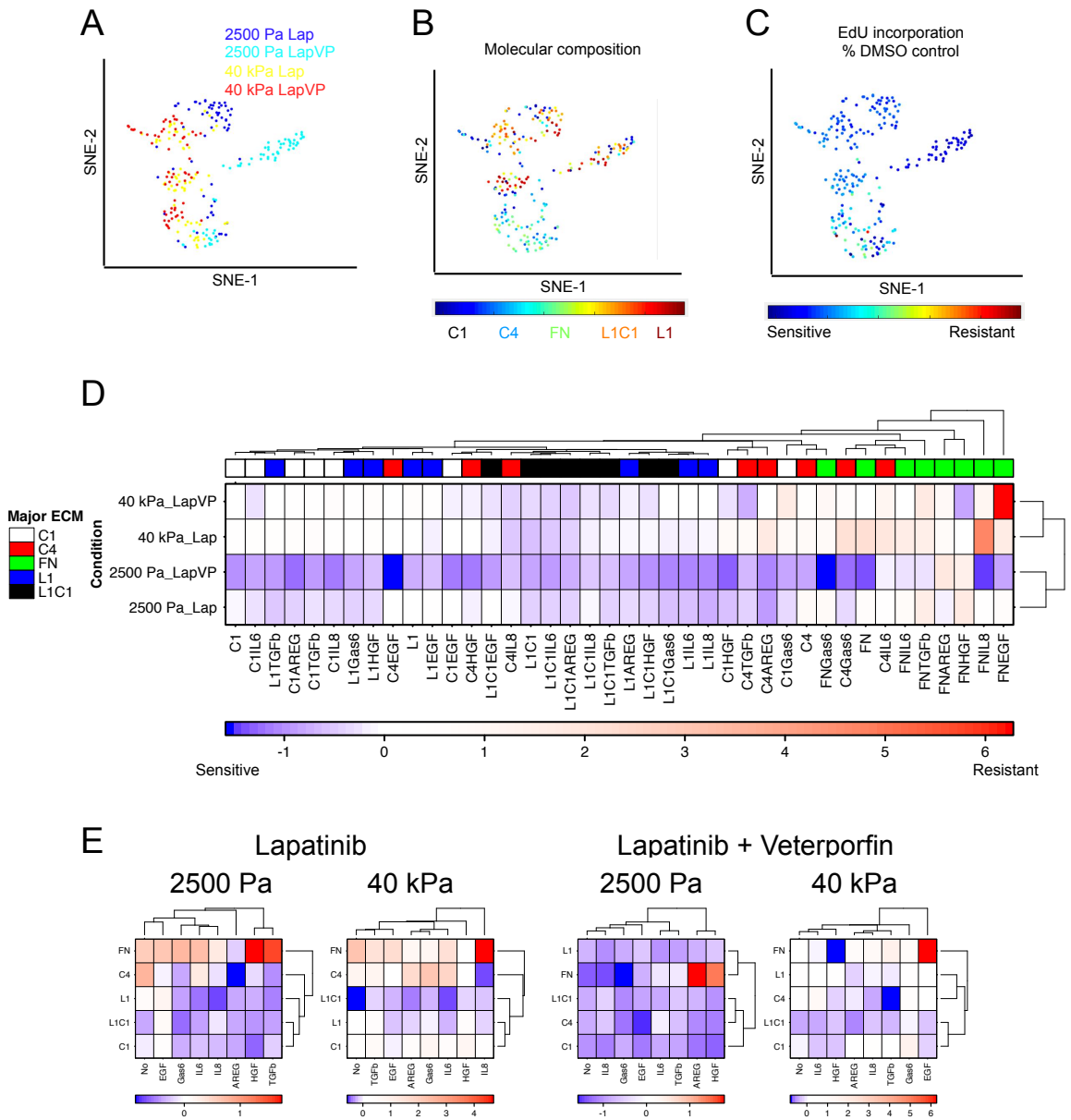
A
2500 Pa Lap
2500 Pa LapVP
40 kPa Lap
40 kPa LapVP
SNE-2
SNE-1
B
Molecular composition
SNE-2
SNE-1
C1 C4 FN L1C1 L1
C
EdU incorporation
% DMSO control
SNE-2
SNE-1
Sensitive Resistant
D
Major ECM
C1
C4
FN
L1
L1C1
Condition
40 kPa_LapVP
40 kPa_Lap
2500 Pa_LapVP
2500 Pa_Lap
C1 C1IL6 L1TGFb C1AREG C1TGFb C1IL8 L1Gas6 L1HGF C4EGF L1 L1EGF C1EGF C4HGF L1C1EGF C4IL8 L1C1 L1C1IL6 L1C1AREG L1C1IL8 L1C1TGFb L1AREG L1C1HGF L1C1Gas6 L1IL6 L1IL8 C1HGF C4TGFb C4AREG C1Gas6 C4 FNGas6 C4Gas6 FN C4IL6 FNIL6 FNTGFb FNAREG FNHGF FNIL8 FNEGF
-1 0 1 2 3 4 5 6
Sensitive Resistant
E
Lapatinib
2500 Pa
40 kPa
Lapatinib + Veterporfin
2500 Pa
40 kPa

Figure 19. A systematic analysis of the microenvironmental impact on drug responses.

A bar graph showing the individual effect of (A) recombinant protein, (B) drug treatment, (C) Major ECM, and (D) matrix rigidity in drug responses. White bar represents control and the dash line represents overall mean. (E~H) Heat maps showing the effect of pair-wised interactions between each individual element of microenvironment to drug responses.

Figure 19

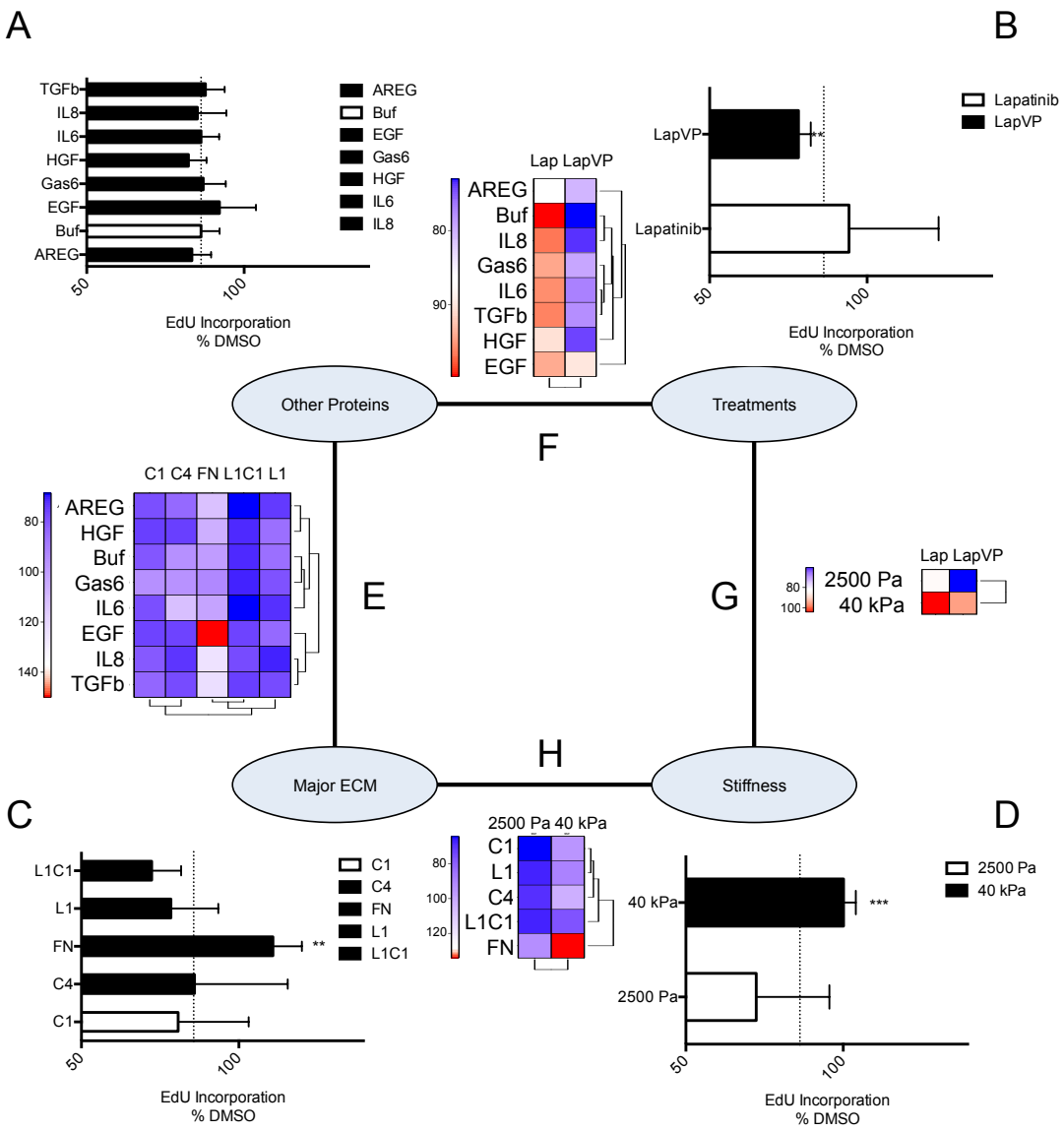
A
B
TGFb
IL8
IL6
HGF
Gas6
EGF
Buf
AREG
AREG
Buf
EGF
Gas6
HGF
IL6
IL8
50
100
EdU Incorporation
% DMSO
Lap LapVP
AREG
Buf
IL8
Gas6
IL6
TGFb
HGF
EGF
80
90
LapVP
Lapatinib
**
Lapatinib
LapVP
50
100
EdU Incorporation
% DMSO
Other Proteins
Treatments
F
C1 C4 FN L1C1 L1
AREG
HGF
Buf
Gas6
IL6
EGF
IL8
TGFb
80
100
120
140
E
G
Lap LapVP
2500 Pa
40 kPa
80
100
H
Major ECM
Stiffness
C
D
L1C1
L1
FN
C4
C1
**
C1
C4
FN
L1
L1C1
50
100
EdU Incorporation
% DMSO
2500 Pa 40 kPa
C1
L1
C4
L1C1
FN
80
100
120
40 kPa
2500 Pa
***
2500 Pa
40 kPa
50
100
EdU Incorporation
% DMSO

Figure 20. The pHER2/HER2 status is affected by microenvironment and contributes to lapatinib inhibition.

(A) The HER2 and pHER2 level of HCC1569 cultured on type 1 collagen coated PA gels with various matrix rigidity were measured by flow cytometry. (B) The pHER2/HER2 status is plotted against lapatinib responses. (C) A box plot showing all data points of lapatinib responses from all combinatorial microenvironments. (D) A box plot showing all data points of pHER2/HER2 status from all combinatorial microenvironments. (E) A linear regression plot showing the correlation between pHER2/HER2 status and lapatinib responses normalized by cells cultured on 2500 Pa gels. (F) A waterfall plot showing the pHER2/HER2 status of all combinatorial microenvironments. (G) A column plot with the same order of labels on x-axis as (F) showing the lapatinib responses of all combinatorial microenvironments.

Figure 20

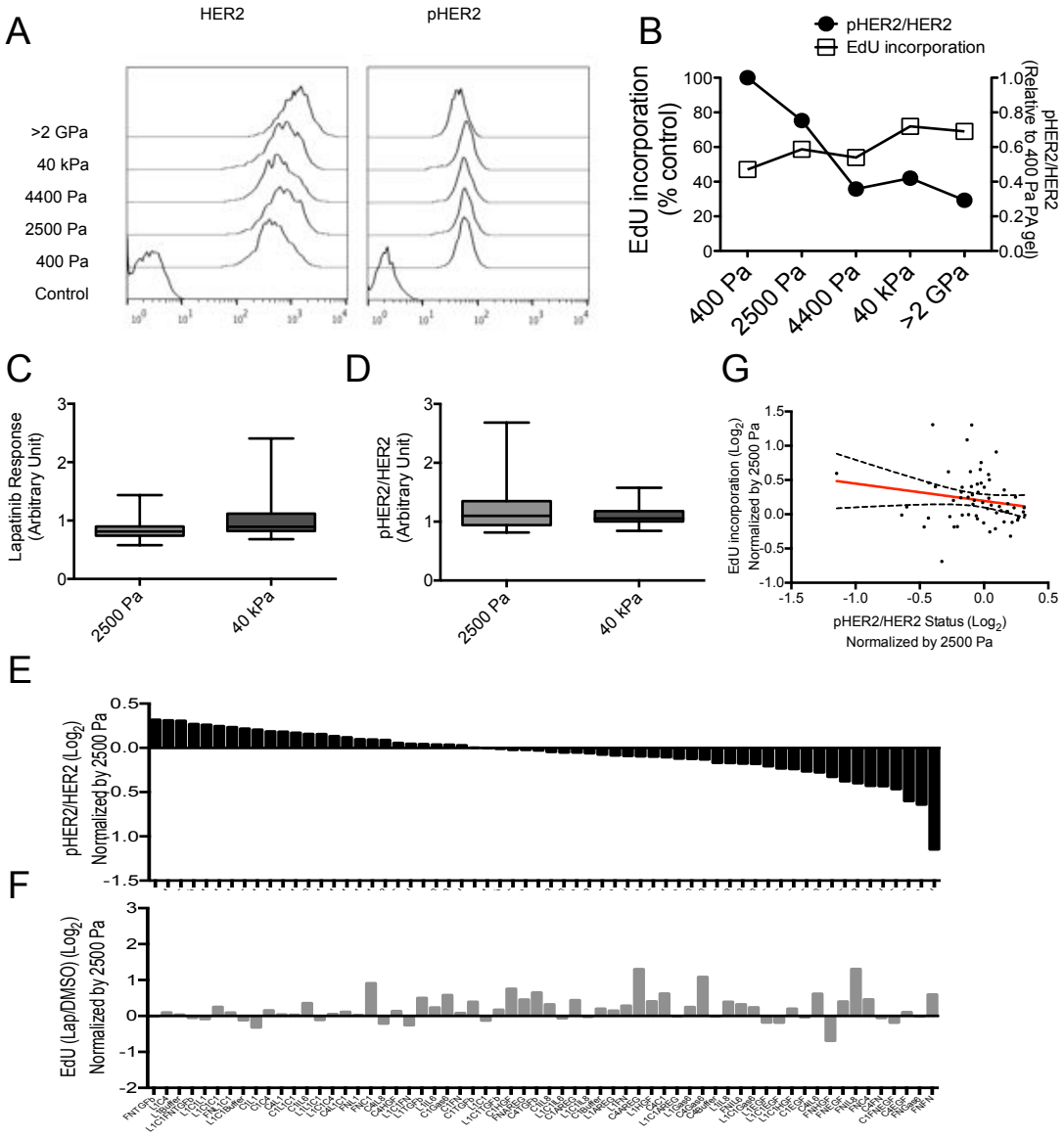
A
HER2
pHER2
>2 GPa
40 kPa
4400 Pa
2500 Pa
400 Pa
Control
B
pHER2/HER2
EdU incorporation
EdU incorporation (% control)
pHER2/HER2 (Relative to 400 Pa PA gel)
400 Pa
2500 Pa
4400 Pa
40 kPa
>2 GPa
C
Lapatinib Response (Arbitrary Unit)
2500 Pa
40 kPa
D
pHER2/HER2 (Arbitrary Unit)
2500 Pa
40 kPa
G
EdU incorporation (Log2) Normalized by 2500 Pa
pHER2/HER2 Status (Log2) Normalized by 2500 Pa
E
pHER2/HER2 (Log2) Normalized by 2500 Pa
F
EdU (Lap/DMSO) (Log2) Normalized by 2500 Pa

Figure 21. Fibronectin conferred lapatinib resistance.

(A) A bar graph showing the relative incorporation of EdU in HCC1569 cultured on either type I collagen or fibronectin coating PA gels, and treated with lapatinib (1.5 μM) for 48 hr. (B) A bar graph showing the proportions of single cells in which YAP and TAZ were located in the nucleus, cytoplasm, or evenly distributed in both compartments, as a function of stiffness and substrate-coating proteins. (C) The plot showing the correlations between *YAP1* and *FN1* gene expression from TCGA dataset (AgilentG4502A_07_3). (D) The plot showing the correlation between YAP and fibronectin protein level from TCPA dataset (BRCA protein RBN). (E) A Kaplan-Meier plot showing the comparison of survival rate between low and high *FN1* gene expression level. (AgilentG4502A_07_3) (F) A Kaplan-Meier plot showing the comparison of survival rate between low and high fibronectin protein level (BRCA protein RBN).

Figure 21

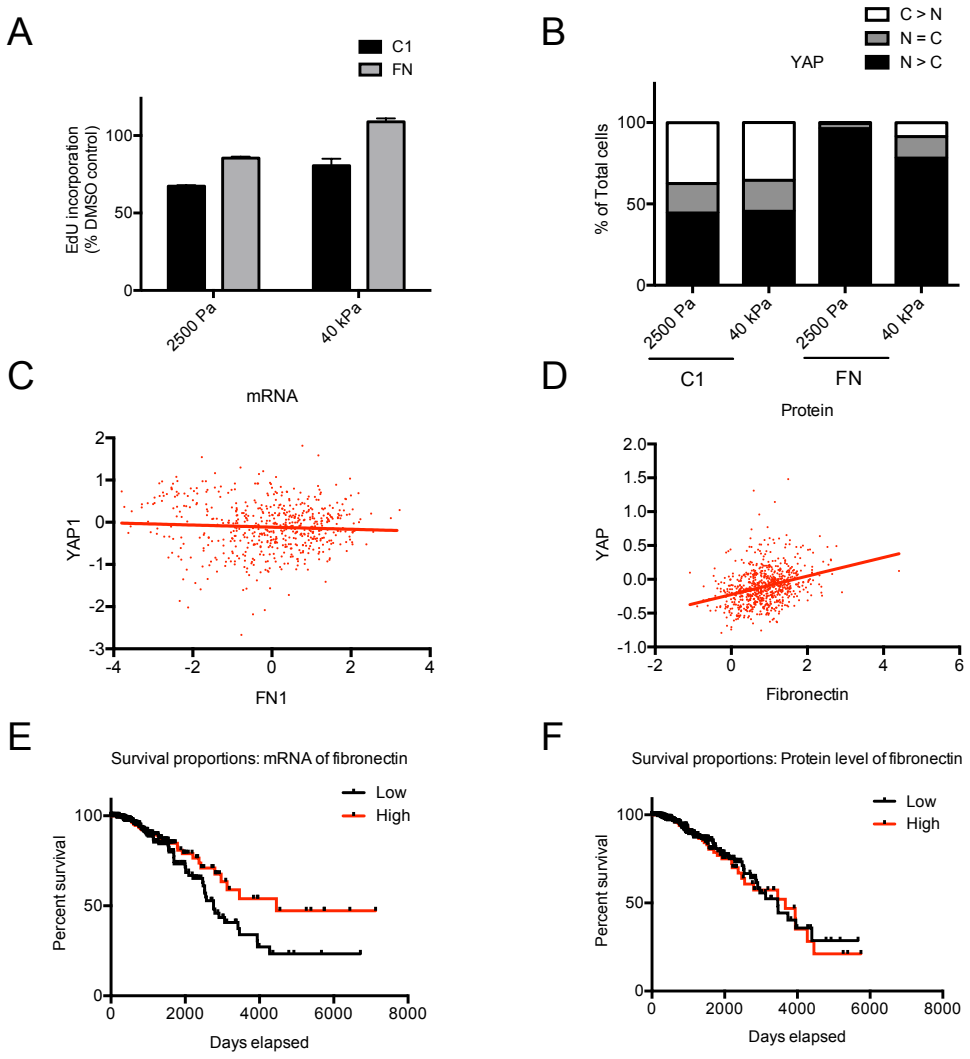
A
C1
FN
EdU incorporation (% DMSO control)
100
50
0
2500 Pa
40 kPa
B
C > N
N = C
N > C
YAP
% of Total cells
100
50
0
2500 Pa
40 kPa
2500 Pa
40 kPa
C1
FN
C
mRNA
YAP1
2
1
0
-1
-2
-3
-4
-2
0
2
4
FN1
D
Protein
YAP
2.0
1.5
1.0
0.5
0.0
-0.5
-1.0
-2
0
2
4
6
Fibronectin
E
Survival proportions: mRNA of fibronectin
Low
High
Percent survival
100
50
0
0
2000
4000
6000
8000
Days elapsed
F
Survival proportions: Protein level of fibronectin
Low
High
Percent survival
100
50
0
0
2000
4000
6000
8000
Days elapsed

Figure 22. Example of MEArray platforms.

(A-E) Representative schemes of MEArray platform and a summary table below.

Figure 22

A B C

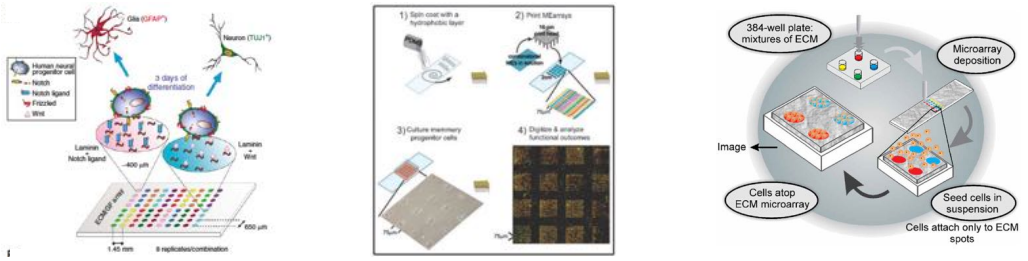

D

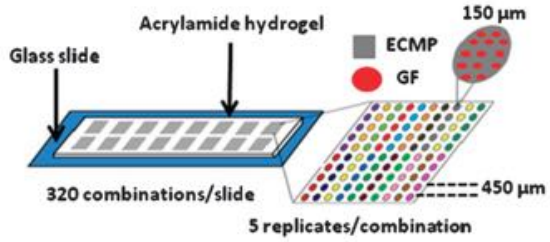

E

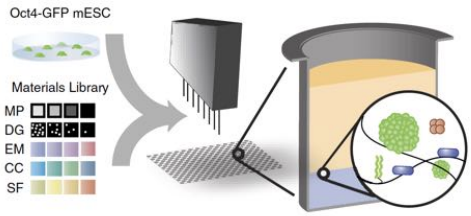

	Tested Applications	Cell type	Modulated Properties	Comments	Ref
A	Cell differentiation	Human neural progenitor cells	2D, molecular composition.	Aldehyde modified glass slide surface for 2D culture. No control of physical properties.	1
B	Cell differentiation, Self-renewal, proliferation.	Human mammary progenitor cells	2D, molecular composition, and rigidity.	PDMS or PA coated slide surfaces for 2D cultures.	2, 3
C	Cell differentiation	Rat hepatocytes	2D, molecular composition.	PEG Hydrogel coated slide surfaces for 2D culture. Lacked of control of physical properties.	4
D	Proliferation and protein activation	Human hepatic stellate cells	2D, molecular composition.	PA gel coated slide surface for 2D culture. Lack of control of physical property.	5
E	Self-renewal	Mouse embryonic stem cells	3D, molecular composition, rigidity, porosity, and degradability.	Modified PEG gel coated wells for 3D culture. Labor intensive and difficult 3D imaging environment.	6

1. Yoav Soen et al. Mol Syst Biol 2006
2. Mark A. LaBarge et al. Integrative Biology 2009
3. Lin etal JoVE….
4. Christopher J Flaim et al. Nature Methods 2005
5. David A. Brafman et al. Integrative Biology 2009
6. A. Ranga et al. Nature Communications 2014

Table 1. Software for processing microarray data.

ImageJ	Image processing	Easy to use, batch processing.	Needs Java to improve automation.
Fiji (ImageJ 2)	Image processing	Built-in plugins specifically for biological data, batch processing.	Needs Java to improve automation.
CellProfiler	Image processing	No coding needed and better native automation compared to ImageJ or Fiji.	Less customization compared to Matlab.
Matlab	Image processing	Highly customizable for image processing.	Needs intensive coding.
Excel	Data processing	Easy to use and very limited coding needed.	Difficult to process large data sets. Limited visualization choices.
R	Data processing	Handles very large data sets.	Needs intensive coding.
Python	Data processing	Easier to use compared to C ++, and can be integrated with other software, such as R.	Needs intensive coding.

Table 2 Data analysis and visualization techniques used with MEArray-type data.

Methods	Type	Advantages	Limitations	Ref
Z-score	Normalization	Easy to implement even in excel.	Sensitive to outlier values, and less accurate in cases with few cell numbers	[122]
Φ-score	Normalization	Overcomes the limitations of Z-score.	Needs specialized software for implementation, such as R	[123]
Dunnett's test	Statistical test	Overcomes problems with type I errors (false positives) due to multiple comparisons to a single control.	Does not make all pair-wise comparisons	[62]
PCA	Dimension reduction	A simple method to PCA to identify patterns due to variance.	Only reflects linear relationships	[80]
ICA	Filter noise and data separation	An alternative method to identify patterns and filter noise.	Data needs to be non Gaussian distribution and independent to each other.	[140]
IPCA	Filter noise and dimension reduction	A method combined PCA and ICA to identify patterns.	Similar to ICA, certain assumptions are needed.	[130]
SPADE	Visualization	Identifies patterns in high dimensional data.	Lower resolution compared to ViSNE, needs further statistical tests for validation.	[133]
ViSNE	Visualization	Similar to SPADE, but has higher resolution. Can reflect non-linear relationships.	Needs further statistical tests for validation.	[81]

Chapter 8: Appendices

Abbreviations

Akt: Protein kinase B

AREG: Amphiregulin

AUC: Area under curve

Axl: Ark and Ufo

BM: Basement membrane

EGFR: Epidermal growth factor receptor

E(Pa): Elastic(Pascal)

HER2: Human epidermal growth factor receptor 2

HER3: Human epidermal growth factor receptor 3

HGF: Hepatocyte growth factor

ICA: Independent component analysis

IPCA: Independent principle component analysis

IPTG: Isopropyl β-D-1-thiogalactopyranoside

MEArray: Microenvironments microarray

MET: Hepatocyte growth factor receptor

PA: Polyacrylamide

PCA: Principle component analysis

PDMS: Polydimethylsiloxane

PEG: Poly(ethylene glycol)

PFA: Paraformaldehyde

RTK: Receptor tyrosine kinase

Sulfo-SANPAH: sulfosuccinimidyl 6-(4'-azido-2'-nitrophenylamino)hexanoate

TAZ: PDZ-binding motif

TCP: Tissue culture plastic

TEAD: Transcription enhancer factor TEF 1

YAP: Yes-associated protein 1